Baryogenesis and leptogenesis from supercooled confinement

Maximilian Dichtl,[a,b] **Jacopo Nava** ⓘ,[b,c] **Silvia Pascoli** ⓘ[b,c] **and Filippo Sala** ⓘ[b,c,1]

[a]*LPTHE, CNRS & Sorbonne Université,*
4 Place Jussieu, F-75252, Paris, France
[b]*Dipartimento di Fisica e Astronomia, Università di Bologna,*
via Irnerio 46, 40126 Bologna, Italy
[c]*INFN, Sezione di Bologna,*
viale Berti Pichat 6/2, 40127 Bologna, Italy

E-mail: maximilian.dichtl@lpthe.jussieu.fr, jacopo.nava2@unibo.it,
silvia.pascoli@unibo.it, f.sala@unibo.it

ABSTRACT: We propose a framework of baryogenesis and leptogenesis that relies on a supercooled confining phase transition (PT) in the early universe. The baryon or lepton asymmetry is sourced by decays of hadrons of the strong dynamics after the PT, and it is enhanced compared to the non-confining case, which was the only one explored so far. This widens the energy range of the PT, where the observed baryon asymmetry can be reproduced, down to the electroweak scale. The framework then becomes testable with gravity waves (GW) at LISA and the Einstein Telescope. We then study two explicit realisations: one of leptogenesis from composite sterile neutrinos that realises inverse see-saw; one of baryogenesis from composite scalars that is partly testable by existing colliders and flavour factories.

---

[1]On leave of absence from LPTHE, CNRS & Sorbonne Université, Paris, France.

Contents

1 Introduction

The universe contains way more matter than antimatter. Independent measurements of the number density n_b of baryons (i.e. particles with a non-zero baryon number B) with the cosmic microwave background [1] and big bang nucleosynthesis [2], combined with the lack of evidence for primordial antibaryons [3, 4], imply a baryon asymmetry of the universe (BAU)

$$Y_{\text{BAU}} \equiv (n_b - n_{\bar{b}})/s \simeq 8.6 \times 10^{-11} \,, \tag{1.1}$$

where s is the entropy density. The Standard Model of particle physics (SM), when combined with the standard cosmological model ΛCDM, clashes with the observed BAU (see e.g. [5])

unless one imposes it as an ad-hoc initial condition, a possibility which becomes untenable when combined with the inflationary paradigm. The BAU is then a strong observational motivation for physics beyond the SM.

To possibly reproduce the observed BAU, one needs processes in the early universe which, at the same time [6]: i) violate of course B; ii) violate also C and CP, otherwise any non-zero B in their final state would be compensated by a $-B$ in the final state of the conjugate process; iii) are out of equilibrium, otherwise the reverse processes would wash-out the baryon asymmetry. Cosmological first order phase transitions (PTs) satisfy condition iii), so that they can potentially explain the BAU if they are accompanied by processes that violate B, C and CP. While first-order PTs in the early universe are not predicted by the SM in isolation [7, 8], they are by many SM extensions motivated by open theoretical problems, see e.g. [9–16]. The proposal of electroweak baryogenesis, for example, relies exactly on new physics that makes the EW PT first-order, see [17] for a recent review.

First-order PTs with fast bubble walls, in particular, are currently receiving massive attention because they produce gravitational waves (GW) [18, 19] observable at current [20–22] and foreseen [23] telescopes. In addition to detectability in GW, first-order PTs with fast walls are motivated as production mechanisms of dark matter (DM) in the form of very heavy particles [24–29] or primordial black holes [30–33]. PTs with fast bubble walls offer also viable mechanisms to explain the baryon asymmetry, see e.g. [34–36]. A particularly simple possibility is to obtain the BAU from out-of-equilibrium decays of particles that obtain their mass at a supercooled PT, as proposed in [36] and worked out so far only for PTs of weakly coupled theories. This mechanism, however, works only for scales of the PT above about 10^8 GeV (see e.g. also [37, 38]), so that it is not testable in any laboratory experiment and only poorly so by GW telescopes, given that the predicted GW are at very high frequencies.

In this paper we point out that, if the supercooled PT is a confining one, then with respect to analogous weakly-coupled PTs, both the yield of the mass-gaining particles (i.e. the hadrons) is larger and wash-out processes are suppressed. We find that these ingredients allow to generate the baryon asymmetry down to PT scales in the TeV range, via hadron's decays. This opens up the possibility to generically test this framework with LISA and the Einstein Telescope. Depending on its specific realisation, we find that this also allows to test the scenario at colliders and/or to connect leptogenesis with neutrino mass generation in a new framework.

2 Framework for the generation of the baryon asymmetry

2.1 Supercooled confining phase transitions

As the temperature of the early universe bath drops, the vacuum state of the theory that is energetically favoured can change, triggering a PT. If the PT is first order it proceeds via nucleation of bubbles of the new ('true') vacuum in the bath, see e.g. [39, 40] for reviews.

A first-order phase transition in the early universe is controlled by the interplay between the energy density of radiation and the difference ΔV between the ones of the old ('false') and new vacuum. The latter is given by

$$\Delta V \equiv c_{\text{vac}} f^4, \tag{2.1}$$

where f is the vacuum expectation value (VEV) of the order parameter ϕ of the phase transition in the true vacuum (which we will later identify with the dilaton), and $c_{\rm vac}$ is a dimensionless, model dependent, quantity parameterizing the vacuum energy difference, typically $c_{\rm vac} \sim \mathcal{O}(1)$ or smaller. The radiation energy density is given by

$$\rho_{\rm rad} = \frac{g_* \pi^2}{30} T^4 \,, \tag{2.2}$$

where g_* counts the effective degrees of freedom of the radiation bath. The phase transition takes place around the nucleation temperature, $T_{\rm nuc}$, when the bubble nucleation rate per unit volume, Γ, becomes comparable to the Hubble parameter H, namely $\Gamma(T_{\rm nuc}) \sim H^4(T_{\rm nuc})$. The PT is said to be supercooled if it happens when the universe is dominated by the vacuum energy rather than by radiation, $\rho_{\rm rad} < \Delta V$, i.e.

$$\text{supercooling:} \qquad T_{\rm nuc} < T_{\rm eq} \equiv \Big(\frac{30 \, c_{\rm vac}}{g_* \pi^2} \Big)^{1/4} f \,, \tag{2.3}$$

where $T_{\rm eq}$ is defined as the temperature when $\rho_{\rm rad} = \Delta V$. Following the phase transition, the order parameter ϕ undergoes oscillations and decays. We assume that its width is comparable or larger than the Hubble rate, so that the universe is reheated to a temperature

$$T_{\rm RH} = \Big(\frac{30 \, c_{\rm vac}}{g_{\rm RH} \pi^2} \Big)^{1/4} f \,, \tag{2.4}$$

where $g_{\rm RH}$ is the number of degrees of freedom in the broken phase that are reheated.

A supercooled PT is generically predicted by potentials $V(\phi)$ that are flat enough at the origin at zero temperature [41], see [42] for a recent systematic study. The needed features of $V(\phi)$ are automatically predicted by models that are approximate scale invariant in the UV, and that spontaneously break scale invariance in the IR, like in radiative generation of IR scales à la Coleman-Weinberg [43, 44].

In this paper we will be interested in strongly coupled realisations, where confinement occurs from the condensation of an approximately conformal strongly-interacting sector, and which are dual to 5D warped models, see e.g. [9–11, 45]. The spontaneous breaking results in a Goldstone boson parametrically lighter than f, the dilaton ϕ, which can be thought of as a condensate of UV quanta of the confining theory. Its potential is generated from a small explicit breaking of scale-invariance in the UV, without which the symmetry could not be spontaneously broken, so that (see e.g. [46])

$$\Delta V = V(\phi = 0) - V(\phi = Zf) \simeq \Big(\frac{Z m_\phi f}{4} \Big)^2 \,, \tag{2.5}$$

where Z is the dilaton's wavefunction renormalization and in strongly coupled theory is expected to be of order one. We clarify that ϕ then denotes the canonically normalized dilaton, and m_ϕ its mass. Eq. (2.5) then implies that m_ϕ and $c_{\rm vac}$ are not independent parameters, but are linked via

$$m_\phi = \frac{4}{Z} c_{\rm vac}^{1/2} f \,. \tag{2.6}$$

$m_\phi < \text{few} \times f$ is enough to achieve values of $T_{\rm nuc}$ orders of magnitude smaller than $T_{\rm eq}$, see e.g. [26, 46]. Larger hierarchies between m_ϕ and f, corresponding to very small values of

$c_{\rm vac}$, may imply that the PT never completes. One could then envisage to complete it via the PT associated to another sector, see [47, 48] for examples where the QCD PT triggers a supercooled EW PT that would otherwise not complete. Obtaining large hierarchies between m_ϕ and f is also non-trivial from the theoretical point of view, see e.g. [49–54] for successful attempts.

2.2 Dynamics of the walls

Supercooled PTs generically predict that bubble walls are ultrarelativistic. As bubbles are nucleated and start to expand, the wall's boost factor γ starts growing as well because the surface tension of the wall loses against the difference in pressures. If nothing prevents their acceleration, then walls 'run away' and γ keeps growing linearly with the bubble radius R.

For the values of $\Delta V/\rho_{\rm rad} \gtrsim 1$ of our interest, plasma effects cannot prevent the walls from becoming faster and faster [55, 56]. Particle physics effects however can. They come from particles obtaining a mass at the wall [57] and radiation from these particles [58], which exert a pressure on the walls and can prevent them from running away. In the context of PTs that are both supercooled and confining, the pressure arises from non-perturbative effects and reads [26]

$$\mathcal{P} \simeq \frac{\zeta(3)}{\pi^2} g_{\rm TC}\, \gamma\, T_{\rm nuc}^3 f\,, \qquad (2.7)$$

where $g_{\rm TC}$ is the number of degrees of freedom, that are charged under the confining group, in the deconfined phase (see the next two subsections). The non-perturbative effects responsible for this pressure can be thought of as the strong-coupling limit of the resummed radiation at the walls in weakly coupled theories, and indeed the pressure associated to the latter effects also scales linearly in γ [59]. Walls then reach a terminal constant boost, $\gamma_{\rm T}$ as soon as $\Delta V = \mathcal{P}$. If this condition is never met, they run away until they collide with walls from other bubbles.

The wall boost factor at bubbles collision then reads

$$\gamma_{\rm coll} \simeq {\rm Min}\Big[\gamma_{\rm run}, \gamma_{\rm T}\Big] \simeq {\rm Min}\Big[1.7\frac{10}{\beta/H}\Big(\frac{0.01}{c_{\rm vac}}\Big)^{1/2}\frac{T_{\rm nuc}}{f}\frac{M_{\rm Pl}}{f}, 10^{-3}\frac{c_{\rm vac}}{0.01}\frac{80}{g_{\rm TC}}\Big(\frac{f}{T_{\rm nuc}}\Big)^3\Big]\,, \qquad (2.8)$$

where the first entry is the runaway value at collision $\gamma_{\rm run} = R_{\rm coll}/(3R_{\rm nuc})$ [59], $R_{\rm coll} = \pi^{1/3}/\beta$ [60] is the typical bubble radius at collision and $R_{\rm nuc}$, of order $T_{\rm nuc}^{-1}$, the one at nucleation. Since in the supercooled PTs of our interest $R_{\rm nuc} \lesssim T_{\rm nuc}^{-1}$ [26], we use $R_{\rm nuc} = T_{\rm nuc}^{-1}/2$ for definiteness (other supercooled PTs may have $R_{\rm nuc} \gtrsim T_{\rm nuc}^{-1}$, see e.g. [61]). We have also introduced the reduced Planck mass $M_{\rm Pl} \simeq 2.4 \times 10^{18}\,{\rm GeV}$ and $\beta \equiv (d\Gamma/dt)\Gamma$, where we remind that Γ is the bubble nucleation rate per unit volume, so that β/H controls the typical number of bubbles per Hubble volume and β/H between 10 and 100 is a typical range for supercooled PTs. Whether the bubble-walls stay in the runaway regime or reach a terminal velocity depends on the amount of supercooling of the PT, which we quantify by the ratio $T_{\rm nuc}/f$. Examining eq. (2.8) it is clear that, in order to have a sufficiently large $\gamma_{\rm coll}$, one needs $T_{\rm nuc} \ll f$.

2.3 Abundance of hadrons

We call hadron any composite state of the confining sector. Hadrons are expected to have a mass $M_{\text{hadr}} \approx 4\pi f \gg T_{\text{nuc}}$ coming from their strong coupling to the dilaton, unless they are lighter for symmetry reasons, like the dilaton itself or other pseudo-goldstone bosons (analogous to pions in QCD). The hadrons do not exist before the PT, where the fundamental 'techniquanta' (TC) are massless (like quarks and gluons in QCD). These are in equilibrium with the thermal bath before the phase transition and their number density to entropy ratio, the Yield, is given by

$$Y_{\text{TC}} \equiv \frac{n_{\text{TC}}}{s} = \frac{45\zeta(3)g_{\text{TC}}}{2\pi^4 g_*}, \tag{2.9}$$

where g_{TC} are the degrees of freedom of the techniquanta and n_{TC} is their number density.

What happens upon the PT was first modeled in [26] and can be summarized as follows. Techniquanta enter the bubble and form fluxtubes that point towards the wall. If techniquanta have more energy than the confinement scale in the wall frame, i.e. if $\gamma T_{\text{nuc}} \gtrsim f$, then these fluxtubes break forming a large number of hadrons, which on average follow the bubble walls in the plasma frame.[1] Fluxtube's breaking also results in the ejection of techniquanta outside the wall, to conserve charge. Both hadrons and ejected particles have very high energies in the bath frame, of order γf. As bubbles expand and collide, hadrons and ejected techniquanta collide with those from other bubbles and with particles of the pre(heated) plasma, whose typical energies are of the order of the dilaton mass m_ϕ. These collisions result in deep inelastic scatterings which ultimately convert the large center of mass energies (of order $m_\phi \gamma f$ in the bath frame) into hadron masses. This conversion has been found by simulations of scatterings and hadronization in [26], and its simplicity makes it pretty robust against the details of this simulation and other possible processes affecting the propagation and scatterings of hadrons and ejected techniquanta [62]. This redistribution of large energies into hadron masses then enhances the yield of hadrons, with respect to that of particles that gain mass at a non-confining PT, by a factor $\gamma_{\text{coll}} f m_\phi / M_{\text{hadr}}^2$. The yield of a given hadron Ψ then reads

$$Y_\Psi \simeq Y_{\text{TC}} \times 3\frac{\gamma_{\text{coll}} f m_\phi}{M_{\text{hadr}}^2} \, Br\big(\text{hadr} \to \Psi\big) \times \Big(\frac{T_{\text{nuc}}}{T_{\text{eq}}}\Big)^3 \frac{T_{\text{RH}}}{T_{\text{eq}}}, \tag{2.10}$$

where $M_{\text{hadr}} \simeq 4\pi f$ and $Br\big(\text{hadr} \to \Psi\big) < 1$ is the number of hadrons Ψ produced over all hadrons in the end of the scattering chains, which is expected to be suppressed if $M_\Psi \gg f$, analogously to QCD. The last factor $(T_{\text{nuc}}/T_{\text{eq}})^3 \, T_{\text{RH}}/T_{\text{eq}} \propto (T_{\text{nuc}}/f)^3$ is the usual dilution of relics from supercooled PTs, the factor $(3\gamma_{\text{coll}} f m_\phi / M_{\text{hadr}}^2)$ is its enhancement specific of confining theories discussed before eq. (2.10).

2.4 Baryon asymmetry from hadrons decay

Let us now assume that a portal connects the confining sector and the SM that results in an otherwise-stable hadron Ψ to decay violating B, C and CP. Note that the portal needs not to necessarily violate C and CP, as their violation could rely on the one existing in the SM

---

[1]Other subtleties can change the picture as c_{vac} and T_{nuc}/f approach 1, but they won't matter for the parameter space of our interest.

(see e.g. [63, 64] for a realisation of this idea in composite Higgs models, although for slow bubble walls) or it could be a property of the strong sector. We do not need to specify this nor the UV origin of the portal in this paper, we just need to know that each of the Ψ or $\bar{\Psi}$ produces on average a net baryon number ϵ_Ψ. The baryon yield then reads

$$Y_B = \epsilon_\Psi \, K_{\mathrm{Sph}} \, Y_\Psi \qquad (2.11)$$

$$\simeq Y_{\mathrm{BAU}} \times \frac{\gamma_{\mathrm{coll}}}{\gamma_{\mathrm{T}}} \frac{\epsilon_\Psi \, K_{\mathrm{Sph}}}{1.2 \cdot 10^{-4}} \frac{Br(\mathrm{hadr} \to \Psi)}{10^{-3} \, Z} \Big(\frac{107.75}{g_{\mathrm{RH}}}\Big)^{\frac{1}{4}} \Big(\frac{c_{\mathrm{vac}}}{0.01}\Big)^{\frac{3}{4}} \Big(\frac{4\pi f}{M_{\mathrm{hadr}}}\Big)^2, \qquad (2.12)$$

where K_{Sph} is the sphaleron reprocessing factor, $K_{\mathrm{Sph}} = 1$ if the baryon asymmetry is generated when electroweak sphalerons are not active, namely when $T \lesssim T_{\mathrm{Sph}} = 132 \, \mathrm{GeV}$ [65], and $K_{\mathrm{Sph}} < 1$ otherwise ($K_{\mathrm{Sph}} = 28/79$ in the SM [66]). In general ϵ_Ψ is at most of order

$$\epsilon_\Psi \lesssim \frac{\mathrm{Im} y^2}{4\pi} \frac{M_\Psi}{\Delta M}, \qquad (2.13)$$

where by $\mathrm{Im} y^2$ we mean the imaginary part of some combination of couplings with coupling dimension 2, and where we include possible enhancements from small hadron mass splittings $\Delta M \ll M_\Psi$. Small hadron mass splittings are actually expected from confining sectors with at least two light quarks (think for example of the neutron and proton masses in QCD).

The discussion so far assumes that the population of hadrons Ψ is unaffected before they decay. First, we estimate the total decay rate of Ψ as $\Gamma_\Psi = C|y|^2 M_\Delta/8\pi$, where C is a model-dependent factor, and observe that they are much faster than the Hubble rate in the entire parameter space that we will consider. So we should compare the rate of Ψ annihilations, i.e. how fast the Ψ want to go to their thermal equilibrium abundance, with Γ_Ψ and not with H. Ψ's annihilate into dilatons ϕ and possibly other particles, depending on the model. As the coupling of Ψ to dilatons is model-independent and large (of order $M_\Psi/(Zf)$), we estimate the annihilation cross section with the analogous QCD one for $p - \bar{p}$ annihilations, $\sigma(\Psi\Psi^* \to \phi\phi)v_{\mathrm{rel}} \sim 4\pi/M_\Psi^2$. Therefore, using eq. (2.12), we obtain the total Ψ annihilation rate

$$\Gamma_{\mathrm{annh}} \sim n_\Psi \sigma v_{\mathrm{rel}} \sim 8.7 \times 10^{-8} M_\Psi \Big(\frac{4\pi f}{M_\Psi}\Big)^5 \frac{\gamma_{\mathrm{coll}}}{\gamma_{\mathrm{T}}} \frac{Br(\mathrm{hadr} \to \Psi)}{0.1 \, Z} \Big(\frac{c_{\mathrm{vac}}}{0.01}\Big)^{\frac{3}{2}} \frac{107.75}{g_{\mathrm{RH}}} \frac{g_*}{200}. \qquad (2.14)$$

In order to not change the abundance of the Ψs before they decay and source the BAU, we require Γ_{annh} to be below $\Gamma_\Psi = C|y|^2 M_\Delta/8\pi$, i.e. the following ratio should be smaller than one:

$$\frac{\Gamma_{\mathrm{annh}}}{\Gamma_\Psi} \simeq \frac{0.02}{C} \times \Big(\frac{0.01}{|y|}\Big)^2 \Big(\frac{4\pi f}{M_\Delta}\Big)^5 \frac{\gamma_{\mathrm{coll}}}{\gamma_{\mathrm{T}}} \frac{Br(\mathrm{hadr} \to \Psi)}{0.1 \, Z} \Big(\frac{c_{\mathrm{vac}}}{0.01}\Big)^{\frac{3}{2}} \frac{107.75}{g_{\mathrm{RH}}} \frac{g_*}{200}. \qquad (2.15)$$

In the regions where this is larger than one, it could still possible to source the BAU, as there is still a population of Ψs. The determination of the BAU would require additional calculations. Since in most of the parameter space of our interest $\Gamma_{\mathrm{annh}} < \Gamma_\Psi$, for simplicity we do not compute the BAU there but just warn the reader whenever we have $\Gamma_{\mathrm{annh}} > \Gamma_\Psi$.

The parameter space where our framework can potentially reproduce the observed BAU is displayed in figure 1 for representative benchmark values of the parameters, for $f \geq \mathrm{MeV}$ cause lower values are excluded by Big Bang Nucleosynthesis (BBN), see e.g. [22]. Imposing
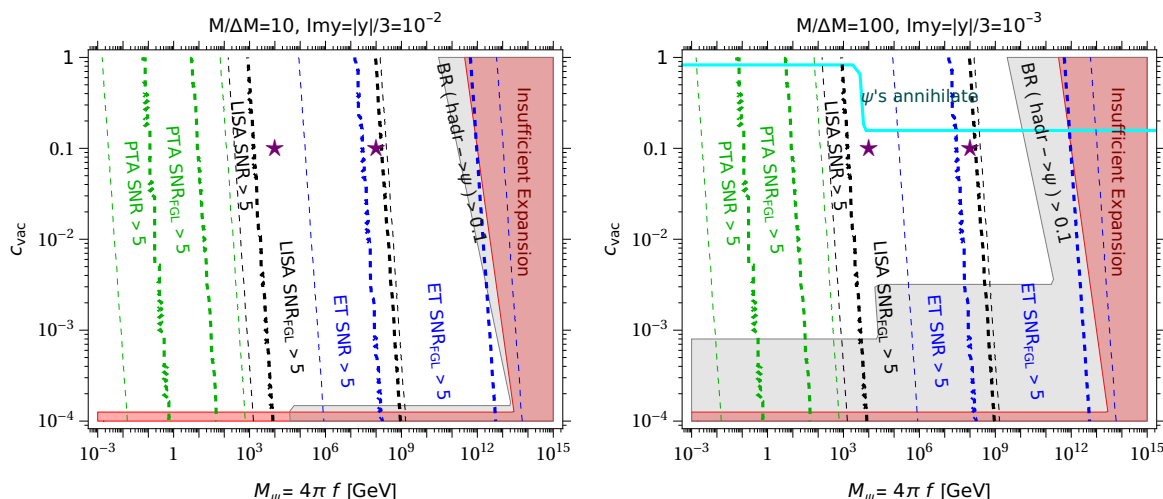
Figure 1. Parameter space where our baryogenesis framework manages to reproduce the observed BAU, and its testability in gravity waves with LISA, the Einstein Telescope and the PTA. We choose $g_{\rm TC} = 80$, $g_* = g_{\rm SM} + g_{\rm TC}$ and, for definiteness, $g_{\rm RH} = g_{\rm SM} + 1$ (where the $+1$ accounts for the dilaton), the dilaton wavefunction normalization $Z = 1$ and $T_{\rm nuc}/f = 10^{-3}$. The white area is allowed by the PT dynamics and can accomodate the baryon asymmetry, where we saturate the baryon yield at each point, by obtaining $Br(\text{hadr} \to \Psi)$ from eq. (2.12). The excluded gray region presents values of $Br(\text{hadr} \to \Psi) > 0.1$, chosen as a benchmark upper limit, hence it cannot account for the whole baryon asymmetry of the Universe. The excluded red region presents $\gamma_{\rm coll} < M_\Psi/T_{\rm nuc}$, hence the hadrons cannot enter the bubble and provide the BAU. Above the cyan lines hadrons start to equilibrate with dilatons before they decay, so the computation of the BAU should be different than the one we employed. The regions delimited by the green, black and blue dashed lines are testable, respectively, by PTAs, LISA and the Einstein Telescope, where the astrophysical foregrounds have (not) been taken into account in the thicker (thinner) lines. We denote with violet stars the two points of the parameter space for which we computed the gravitational wave spectrum shown in figure 2. The viable parameter space will be reduced in specific realizations of our framework, by model-dependent washout effects or laboratory searches depending on the SM interactions of the hadrons Ψ, see figures 6 and 8.

$Y_B = Y_{\rm BAU}$ fixes the value of $Br(\text{hadr} \to \Psi)$ in every point of the parameter space. We require $Br(\text{hadr} \to \Psi) < 0.1$ because string fragmentation is expected to give rise mostly to light hadrons, and at least one light hadron, the dilaton, exists in our picture. We also require $\Gamma_{\rm annh}/\Gamma_\Psi < 1$, for definiteness for $C = 1$ and using $|y|=3\,{\rm Im}y$. As long as the walls are in the terminal velocity regime, Y_B is independent of both f and $T_{\rm nuc}/f$. These parameters play a role as soon as collisions happen in the runaway regime, i.e. in a region of large f and small $T_{\rm nuc}/f$, where Y_B gets quickly suppressed (indeed figure 1 displays that one cannor reproduce the BAU at large f).

f and $T_{\rm nuc}/f$ also play a role in defining the regions where the BAU can be washed out by various effects. Washout effects are not included in eq. (2.12), nor they are visualized in figure 1, because they depend on the specific model realising our framework. One can still identify the following general expectations for them. Concerning inverse decays, they can be neglected as long as $M_\Psi \gg T_{\rm RH}$, because their rate is Boltzmann-suppressed at large $M_\Psi/T_{\rm RH}$. $M_\Psi \gg T_{\rm RH}$ is actually a consequence of $T_{\rm RH} \lesssim f$ (see eq. (2.4)) and $M_\Psi \simeq 4\pi f$. M_Ψ/f is the

hadron coupling to the dilaton, the large values needed to avoid washout from inverse decays can only be obtained in strongly-coupled theories. Other washout processes that generically exist are $2 \to 2$ scatterings mediated by Ψ. Requiring that they are negligible imposes i) an upper bound on $\mathrm{Im}\, y^2$ of eq. (2.13), hence our normalization of ϵ_Ψ in eq. (2.12) to a small number, and ii) an absolute lower limit on M_ψ, because they are suppressed by some power of M_ψ. Condition ii) is what prevents from going to values of f much below a TeV, although it is possible that a minimal model-building effort weakens this requirement. Another obstruction to achieving $f \lesssim \mathrm{TeV}$ arises in models where the confining sector generates a lepton asymmetry, because then one needs $T_{\mathrm{RH}} > T_{\mathrm{Sph}}$ to transmit it to the baryon sector.

Two key features of our framework, that are different with respect to its weakly coupled analogue of [36, 38], can already be grasped by our general discussion so far:

$\diamond$ the hadron yield is enhanced by the strong dynamics and it allows for a larger BAU;

$\diamond$ the strong coupling $M_\Psi/f \gg 1$ suppresses washout coming from inverse decays.

They imply that this mechanism works for scales of the PT down to (at least) the weak scale, which opens the possibility to test it with both LISA and the Einstein Telescope, which is the topic of section 3. It also makes the mechanism testable in the laboratory, either directly producing the hadrons at high-energy colliders, or indirectly testing their CP and flavour violating effects. Finally, a scale of the PT down to (at least) the TeV scale also allows for interesting theoretical connections, e.g. with models explaining the origin of the weak scale, or of neutrino masses, with confining dynamics. We will explore some of these consequences in two explicit models that realise our framework, in sections 4 and 5.

3 Gravitational wave signal

We now detail the expected GW signal from a supercooled PT. Using the numerical results from [67], the GW energy density power spectrum as measured today, for initially thick walled, runaway bubbles is given by

$$h^2 \Omega_{\mathrm{GW}}(\nu) \equiv h^2 \frac{d\, \Omega_{\mathrm{GW}}}{d \log(\nu)} = h^2 \Omega_{\mathrm{rad}}^0 \left(\frac{g_0}{g_{\mathrm{RH}}}\right)^{\frac{1}{3}} \Omega_{\mathrm{GW}}^{\mathrm{PT}}(\nu) \simeq 4.4 \times 10^{-7} \left(\frac{100}{g_{\mathrm{RH}}}\right)^{\frac{1}{3}} \left(\frac{\alpha_{\mathrm{GW}}}{1+\alpha_{\mathrm{GW}}}\right)^2 \frac{S_\phi(\nu)}{(\beta/H)^2},$$
(3.1)

where $h \simeq 0.67$ is the dimensionless Hubble parameter as determined by Planck [1]. In eq. (3.1) the factors Ω_{rad}^0 and $(g_0/g_{\mathrm{RH}})^{\frac{1}{3}}$ take into account that the GW energy density redshifts as radiation from its value at the PT, $\Omega_{\mathrm{GW}}^{\mathrm{PT}}$, until today, and Ω_{rad}^0 and g_0 are, respectively, the energy fraction in radiation and the degrees of freedom in entropy today. α_{GW} is the energy released as bulk motion during the PT (which we approximate as the energy difference between the false and true vacuum, ΔV) normalized to the radiation density ρ_{rad}, namely

$$\alpha_{\mathrm{GW}} \simeq \frac{\Delta V}{\rho_{\mathrm{rad}}} = \left(\frac{T_{\mathrm{eq}}}{T_{\mathrm{nuc}}}\right)^4 = \frac{30 c_{\mathrm{vac}}}{\pi^2 g^*} \left(\frac{f}{T_{\mathrm{nuc}}}\right)^4,$$
(3.2)

thus one expects $\alpha_{\mathrm{GW}} \gg 1$ for supercooled PTs. The shape of the spectrum is governed by the spectral function

$$S_\phi(\nu) = \frac{(a+b)\tilde{\nu}^b \nu^a}{b\, \tilde{\nu}^{(a+b)} + a\, \nu^{(a+b)}},$$
(3.3)

where we adopt the central values for the bubbles in the setup with the thickest walls from [67], namely $\{a, b\} = \{0.742, 2.16\}$. The peak frequency of the signal today is given by

$$\tilde{\nu} = 33\,\mu\text{Hz} \left(\frac{g_{\text{RH}}}{100}\right)^{1/6} (\beta/H) \left(\frac{T_{\text{RH}}}{10^3\,\text{GeV}}\right). \tag{3.4}$$

Finally, one should impose that $\Omega_{\text{GW}} \propto \nu^3$ at small frequencies, due to causality for super-horizon modes at GW production [68]. We therefore apply a cut in the spectrum at the redshifted frequency today of

$$\nu^*(t_0) = \frac{a(T_{\text{RH}})}{a_0} \frac{H(T_{\text{RH}})}{2\pi}, \tag{3.5}$$

below which we enforce the correct IR scaling and where $a(T_{\text{RH}})/a_0$ is the ratio of the scale factors between the PT and today.

The numerical simulations performed in [67] assume that bubbles effectively runaway until collision, however a large part of our parameter space, notably the one associated to a PT around the TeV scale, sits in the terminal velocity regime, where the vacuum energy pressure is counterbalanced by the friction produced by particles in the plasma. The vacuum energy is thus partly converted into kinetic energy of the particles in the plasma already prior to the bubble wall collision. However, the contribution from sound waves or turbulence [69, 70] in supercooled PTs is not yet clearly understood. Indeed, current hydrodynamical simulations, which aim to capture the contribution of the bulk motion of the plasma to the GW signal, do not yet extend into the regime in which the energy density in radiation is subdominant to the vacuum [71] and analytical studies of shock-waves in the relativistic limit have just started [72]. In this scenario one can argue that derivatives of the envelope approximation such as the so-called bulk flow model are more realistic in modelling the GW signal.

In practice, the difference between [67] and bulk-flow models like [73] is very mild, see e.g. the comparison in [61]. Therefore we use the parametrization from [67], described above, for both regimes of wall velocities. Examples of GW spectra are shown in figure 2, for $\alpha_{\text{GW}} = 100$ and $\beta/H = 15$, both typical of supercooled PTs and for two benchmark values of c_{vac} and M_Ψ.

Our model can be probed by several current or upcoming GW interferometers, due to the wide parameter space allowed. The sensitivity of a detector to a GW signal is given by

$$\Omega_{\text{sens}}(\nu) = \frac{4\pi^2}{3H_0^2} \nu^3 S_n(\nu), \tag{3.6}$$

where $H_0 = 100h$ km/s/Mpc is the present day Hubble parameter and S_n is the noise spectral density [74]. The signal to noise ratio SNR to a GW background is given in terms of the above quantities as [75]

$$\text{SNR} = \sqrt{t \int_{\nu_{\text{min}}}^{\nu_{\text{max}}} d\nu \left(\frac{\Omega_{\text{GW}}(\nu)}{\Omega_{\text{sens}}(\nu)}\right)^2}, \tag{3.7}$$

where $\nu_{\text{min}}, \nu_{\text{max}}$ and t denotes the minimal and maximal frequencies accessible at the detector and the fiducial observation time, which is taken to be $t = 10$ years for the ET and $t = 3$ years for LISA. Using this expression, the so called power-law-integrated (PLI) sensitivity curves are computed [75], and our calculations for the PLI sensitivity curves of, LISA [76],
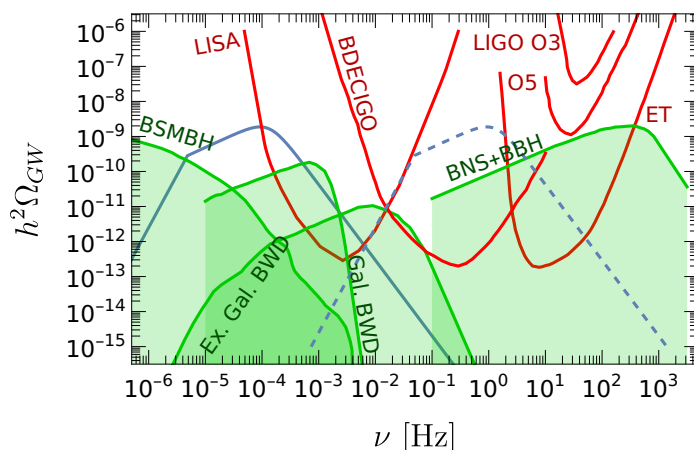
Figure 2. Example of GW spectra for two benchmark points of the $\{c_{\mathrm{vac}}, M_\Psi\}$ parameter space. The solid (dashed) blue line shows the predicted gravitational wave spectrum for the PT, with $\{c_{\mathrm{vac}}, M_\Psi\} = \{10^{-1}, 10^4 \text{ GeV}\}$ and $\{c_{\mathrm{vac}}, M_\Psi\} = \{10^{-1}, 10^8 \text{ GeV}\}$. We have assumed $T_{\mathrm{nuc}}/f = 10^{-3}$, $\alpha_{\mathrm{GW}} = 100$ and $\beta/H = 15$ as typical benchmark values for supercooled PTs. The spectra are compared with PLI sensitivity curves, shown as red lines, with signal-to-noise ratio SNR=10 for LISA [76] and the Einstein Telescope (ET) [79]. We also show PLI sensitivity curves for LIGO-VIRGO O3, LIGO-VIRGO Design A+ sensitivity [78] and BDECIGO [77]. Estimated astrophysical foregrounds from binary super-massive black holes [80], galactic white-dwarf binaries [81], extragalactic white-dwarf binaries [82], binary black holes and neutron stars [78] are also shown as green shaded regions.

BDECIGO [77], LIGO-VIRGO-KAGRA [78] and Einstein Telescope (ET) [79] (configuration '2L 0° 20km' for definiteness) are shown in figure 2, for a fiducial choice of SNR=10.

There are several astrophysical stochastic GW foregrounds which could mimic the GW signal coming from the PT, see figure 2 for details. In order to take this limitation into account we also define a foreground-limited signal to noise ratio $\mathrm{SNR_{FGL}}$,

$$\mathrm{SNR_{FGL}} = \sqrt{T \int_{\nu_{\min}}^{\nu_{\max}} d\nu \Big(\frac{\mathrm{Max}[\Omega_{\mathrm{GW}}(\nu) - \Omega_{FG}(\nu), 0]}{\Omega_{\mathrm{sens}}(\nu)} \Big)^2}. \tag{3.8}$$

With the above conservative definition we impose that our signal is not detectable if buried under the astrophysical foreground $\Omega_{FG}(\nu)$. We show in figure 1 the regions of parameter space of our BAU framework that could be probed by Pulsar Timing Arrays (PTA), LISA and the ET, which we define as those where $\mathrm{SNR_{FGL}} \geq 5$. For comparison, we also show the regions that one could probe in absence of astrophysical foregrounds, which could be relevant in case one will envisage ways to tell them apart from a GW signal from PTs. The two sensitivities are anyway very similar for LISA, due to the strong GW signal from the PT in comparison with foregrounds, while for PTAs and ET we find an appreciable difference. The sensitivity showing up for $f \lesssim 100 \,\mathrm{GeV}$ is the one attainable using GWs as measured by PTA, which we compute following [83] and identifies yet another way to test our framework, in case one manages to make it work down to such small scales of the PT. If one did, then one could potentially explain the GW background observed by PTAs [84–87] with a PT [88, 89] that, at the same time, explains the BAU via the framework proposed in this paper. In any case, a very large fraction of the allowed space could indeed be probed by GW interferometers.

4   Model 1: baryogenesis from a composite scalar

We have so far discussed a general framework for the generation of the baryon asymmetry and we have established that it presents some interesting features, as an enhanced production of the baryon yield with respect to the non-confining case and a gravitational wave signal potentially in reach of current and future GW interferometers. We now specify our framework to two models already discussed in the literature, compute their predictions for washout and for the BAU as well as for detection, and show explicitly that we can extend significantly their allowed parameter space for a successful baryogenesis/leptogenesis.

### 4.1   Model and baryon asymmetry

We start by revisiting the model of baryogenesis discussed in [36], where the baryon number is produced by the CP-violating decays of a heavy scalar denoted there as Δ. In our setup Δ is a composite scalar field originating from a dark confining sector and it is a realization of the Ψ hadron discussed above. We introduce $i = 1, 2$ generations of the Δ_i scalars, with $M_{\Delta_2} > M_{\Delta_1}$. We assume these fields to transform as $(3, 1, 2/3)$ under the SM gauge group $\mathrm{SU(3)_c} \times \mathrm{SU(2)_L} \times \mathrm{U(1)_Y}$. We also introduce a SM gauge singlet fermion χ with mass M_χ and the following baryon number violating Yukawa interactions of Δ_i:

$$\mathcal{L} \supset y_{di} \Delta_i \overline{d_R^c} d_R + y_{ui} \Delta_i \overline{\chi_R} u_R^c + \mathrm{h.c.}, \tag{4.1}$$

where colour indices have been suppressed for simplicity of the notation. y_{di} is antisymmetric in flavour d as a consequence of the antisymmetry of the colour indices. A necessary condition for CP violation is that the above couplings should be complex. Some, but not all the phases, even in the minimal scenario, can be removed through field rephasings $f \to e^{i\alpha_f} f$. To be more concrete let's examine some specific scenarios:

⬦ In the minimal scenario there is only one copy of χ and the $\Delta_{1,2}$ couple each to one up-type quark and to a pair of down-type quarks (that do not have the same flavour). This results in 4 Yukawa couplings y. One can remove 3 out of their 4 phases by rephasing the Δ_i and χ, but one phase survives since in general $\mathrm{Arg}(y_{d2}) - \mathrm{Arg}(y_{d1}) \neq \mathrm{Arg}(y_{u2}) - \mathrm{Arg}(y_{u1})$. Thus in this setup there are 4 couplings and 1 (physical) phase.

⬦ One can switch on all the allowed SM quark Yukawa couplings, keeping a single copy of χ. This setup features 12 couplings, 6 involving down-type quarks and 6 involving the up-type quarks. As in the previous case we can rephase the 3 new fields, so we're left with 9 independent new phases.

⬦ For 3 copies of χ, we find 24 couplings (6 from down- and 18 from up-type quarks). With respect to the previous setup we have the freedom to remove 2 more phases by redefining $\chi_{2,3}$, therefore we end up with 19 independent phases.

Note that in the second and third case (but not the first one) one could remove further phases from the Yukawa couplings of eq. (4.1) by rephasing the right-handed quarks, but those phases would not be unphysical as they would show up in the quark Yukawas.
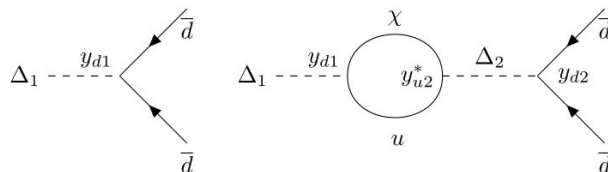
Figure 3. Example of the diagrams which interfere and lead to CP violation. The intermediate loop particles are kinematically able to go on-shell.

Assuming $M_\chi \ll M_{\Delta_i}$ to avoid complications with phase space effects, the couplings of the Lagrangian eq. (4.1) lead to the following tree level decay rates for the scalars Δ_i

$$\Gamma(\Delta_i \to \overline{d_R d'_R}) \simeq \frac{|y_{di}|^2}{8\pi} M_{\Delta_i}, \tag{4.2}$$

$$\Gamma(\Delta_i \to \chi u_R) \simeq \frac{|y_{ui}|^2}{16\pi} M_{\Delta_i}, \tag{4.3}$$

where by d'_R we denote a right down quark of different flavour than d_R, we have not summed over flavours and we have summed over final state colours for the first decay. Interference between tree- and loop-level diagrams, as those shown in figure 3, leads to CP violation in the decays. Focusing on the decays of Δ_1 only, CP violation can be parametrized as

$$
\begin{aligned}
\Gamma(\Delta_1 \to \overline{d_R d'_R}) &= \Gamma_{1d}(1 + \epsilon_d) \,, \\
\Gamma(\Delta_1^* \to d_R d'_R) &= \Gamma_{1d}(1 - \epsilon_d) \,, \\
\Gamma(\Delta_1 \to \chi u_R) &= \Gamma_{1u}(1 + \epsilon_u) \,, \\
\Gamma(\Delta_1^* \to \overline{\chi u_R}) &= \Gamma_{1u}(1 - \epsilon_u) \,.
\end{aligned}
\tag{4.4}
$$

Since the total decay widths of Δ_1 and Δ_1^* have to be equal due to the CPT theorem, it follows that $\epsilon_d \Gamma_{1d} = -\epsilon_u \Gamma_{1u}$. The imaginary part of the loop in figure 3 controls the rate asymmetry between Δ_1 and Δ_1^* decays and can be extracted via Cutkosky rules [90]. One then finds for the rate asymmetry

$$\epsilon_\Delta = \frac{1}{2\pi} \frac{\text{Im}(y_{d1}^* y_{u1} y_{u2}^* y_{d2})}{|y_{ui}|^2 + 2|y_{di}|^2} \frac{M_{\Delta_1}^2}{M_{\Delta_2}^2 - M_{\Delta_1}^2} \sim \frac{\text{Im}[y^2]}{6\pi} \frac{M_{\Delta_1}^2}{M_{\Delta_2}^2 - M_{\Delta_1}^2} \,, \tag{4.5}$$

where from now on we assume that there is no major hierarchy among the Yukawa couplings y and we take generic $\mathcal{O}(1)$ phases. We are also discarding resonant enhancements of the rate asymmetry, namely we are assuming that $M_{\Delta_2} - M_{\Delta_1} \gg \Gamma_{\Delta_i}$. Finally, the baryon asymmetry is obtained by plugging ϵ_Δ of eq. (4.5) in Y_B of eq. (2.12).

4.2 Washout processes

In our scenario the most constraining washout processes are those occurring after reheating, after the PT. The reason is that the population of the Δ hadrons, yielding the baryon asymmetry via their decays, is mostly sourced by the deep inelastic scatterings of the hadrons (produced upon string fragmentation of incoming or ejected techniquanta) with other hadrons or bath particles. These scatterings mostly happen after bubble percolation, so that washout

effects just after wall crossing, like those considered in [36], are not relevant in our framework (but see the end of the previous subsection for Δ annihilations after percolation).

After bubbles percolate and all hadrons are produced, diquark interactions violating $B - L$ can result in washout if $T_{\rm RH}$ is too high. Off-shell $2 \to 2$ scattering processes mediated by Δ that violate baryon number, e.g. $d\, d' \leftrightarrow \overline{\chi u}$, have a rate that can be estimated as

$$\Gamma_{\rm WO} \simeq \frac{y^4\, T_{\rm RH}^5}{8\pi M_\Delta^4}\,, \tag{4.6}$$

where we are integrating out Δ because $T_{\rm RH} \ll M_\Delta$ in our framework. This rate is harmless for our scenario provided that it is below the Hubble rate H, namely

$$\frac{M_\Delta}{T_{\rm RH}} \geq \Big(\frac{\sqrt{90} y^4 M_{\rm Pl}}{8\pi^2 g^{*1/2} T_{\rm RH}} \Big)^{1/4}\,. \tag{4.7}$$

Moreover, also inverse decays into on-shell Δ can lead to $B - L$ washout. The Boltzmann suppressed rate is given by

$$\Gamma_{ID} \simeq \frac{3\, y^2}{16\pi} M_\Delta \Big(\frac{M_\Delta}{T_{\rm RH}} \Big)^{3/2} {\rm Exp}\Big[-\frac{M_\Delta}{T_{\rm RH}} \Big]\,. \tag{4.8}$$

This is safely below H, provided that

$$\frac{M_\Delta}{T_{\rm RH}} \geq {\rm Log}\Big[\frac{y^2 M_{\rm Pl}}{8\pi\, g^{*1/2} T_{\rm RH}} \Big(\frac{M_\Delta}{T_{\rm RH}} \Big)^{5/2} \Big]\,. \tag{4.9}$$

4.3 Proton decays and further washout from χ

So far we have not addressed the detailed nature of χ, which we assume not to be linked to the confining sector, to allow us more freedom with its phenomenology. A first idea is to take χ to be close to massless, which would be the case if the SM neutrinos gain Dirac mass via a Yukawa-type interaction $y_\nu \overline{L} H \chi_R$, with $y_\nu \sim 10^{-12}$. However, χ allows nucleon decays via t-channel diagrams mediated by Δ, like $p \to K^+ \chi$, as long as $M_\chi < m_p - m_K^+$. Taking the couplings to all the generations to be of the same order, we estimate the decay rate

$$\Gamma(p \to K^+ \chi) \sim \frac{y_u^2 y_d^2}{64\pi^3} \frac{m_p^5}{M_\Delta^4} \simeq \Big(\frac{y}{10^{-2}} \Big)^4 \Big(\frac{\rm TeV}{M_\Delta} \Big)^4 10^{-23}\ {\rm GeV}. \tag{4.10}$$

From the experimental bound on the partial proton lifetime, $\tau(p \to K^+ \nu) > 5.9 \times 10^{33}$ years [91], it follows that $\Gamma(p \to K^+ \nu) < 3.5 \times 10^{-66}\,{\rm GeV}$, therefore a scenario in which $M_\chi < m_p - m_K^+$ would completely rule out our interesting region of the parameter space around the TeV. Considering now the case where $M_\chi > m_p - m_K^+$, a natural assumption would be to assume χ to be Majorana, with a $\frac{1}{2} M_\chi \overline{\chi}_R \chi_R^c$ mass term and to couple it to the SM leptons and the Higgs H via the Yukawa coupling y_ν and provide SM neutrino masses with a standard type-I seesaw. In this case the decay $p \to K^+ \nu$ would receive contribution from y_ν and one can get an estimate for the decay width

$$\Gamma(p \to K^+ \nu) \sim \frac{y_u^2 y_d^2}{64\pi^3} \frac{m_p^5}{M_\Delta^4} \Big(\frac{y_\nu v}{M_\chi} \Big)^2 \simeq \Big(\frac{y}{10^{-2}} \Big)^4 \Big(\frac{\rm TeV}{M_\Delta} \Big)^4 \Big(\frac{\rm TeV}{M_\chi} \Big) 10^{-37}\ {\rm GeV}, \tag{4.11}$$

which again would exclude the most interesting region of our parameter space. Therefore, in order not to spoil the interesting features discussed so far, one needs $M_\chi > m_p - m_K^+$ and to disentangle χ from the generation of neutrino masses, so that the coupling y_ν can be taken as small as needed to respect limits on nucleon's lifetimes, independently of the other parameters.

Moreover, the same couplings in eq. (4.1) which produce the baryon asymmetry in our setup also lead to a partial decay width of χ given by

$$\Gamma(\chi \to \overline{udd'}) = \frac{1}{1024\pi^3} \left| \frac{y_{u1}y_{d1}}{M_{\Delta_1}^2} + \frac{y_{u2}y_{d2}}{M_{\Delta_2}^2} \right|^2 M_\chi^5 . \tag{4.12}$$

After baryogenesis there is an excess of χ over $\overline{\chi}$, thus if χ is Dirac and $M_\chi < M_\Delta$ the asymmetry gets erased exactly once χ decay. Indeed the decays $\chi \to \overline{udd'}$ and $\overline{\chi} \to udd'$ would exactly erase the CP asymmetry, due to $\epsilon_d \Gamma_d = -\epsilon_u \Gamma_u$ following from CPT. Note that $M_\chi \geq M_\Delta$ is not a viable option, because then $\Gamma_u = 0$ and so $\epsilon_d = 0$ via CPT, so one would not generate the baryon asymmetry. Instead, if χ is Majorana then both udd and $\overline{udd}$ decays are allowed and the asymmetry is preserved. However, the asymmetry could be spoiled by inverse decays: any excess of udd or $\overline{udd}$ would go back to χ, that would wash it out upon decaying Assuming no hierarchies among the Yukawas y we get the following ratio between the rate of inverse decays and Hubble:

$$\frac{\Gamma(\overline{udd'} \to \chi)}{H(T = M_\chi)} \simeq \frac{(y_u y_d)^2}{256\pi^3 g^{*1/2}} \frac{\pi}{90^{\frac{1}{2}}} \frac{M_\chi^5}{M_\Delta^4} \frac{M_{\text{Pl}}}{M_\chi^2} \sim 10^{-7} \left(\frac{y}{10^{-2}}\right)^4 \left(\frac{\text{TeV}}{M_\Delta}\right)^4 \left(\frac{M_\chi}{\text{GeV}}\right)^3 , \tag{4.13}$$

where we have evaluated H at $T = M_\chi$ because that is the range of temperatures for which inverse decays are most efficient: for $T \ll M_\chi$, $\Gamma(\overline{udd'} \to \chi)$ would be exponentially suppressed, for $T \gg M_\chi$, H would be enhanced but not $\Gamma(\overline{udd'} \to \chi)$.

To summarize, χ does not alter our results as long as i) to avoid nucleons decays, $M_\chi > m_p - m_K^+$ and its coupling to neutrinos is small enough (so that it cannot play a role in the generation of neutrino masses) and ii) to avoid further washouts, M_χ is Majorana and it is smaller enough than M_Δ to keep $\Gamma(\overline{udd'} \to \chi)/H \ll 1$, see eq. (4.13).

4.4 Signals of the composite scalar Δ in laboratory experiments

4.4.1 Collider searches

As it turns out (see figure 6), one can easily accomodate baryogenesis from supercooled confinement with the scalar Δ around or below the electroweak scale, the properties of these particles can be probed thanks to their signatures in high-energy colliders.

A first lower bound on the mass of Δ comes from the measurement of the decay width of the Z boson performed at LEP [92]. Since Δ interacts weakly due to its U(1)$_Y$ charge, it can contribute to the Z boson width, provided that $M_\Delta < M_Z/2$. We compute the following expression for the decay width of Z into a $\Delta\Delta^*$ pair

$$\Gamma(Z \to \Delta\Delta^*) = \frac{3}{16\pi} \left(\frac{2g \sin^2\theta_W}{3\cos\theta_W}\right)^2 M_Z \left(1 - \frac{4M_\Delta^2}{M_Z^2}\right)^{3/2} . \tag{4.14}$$

Since this value is orders of magnitude larger than the uncertainty on the Z boson width, we exclude $M_\Delta < 45\,\text{GeV}$.

Then one can note that Δ has the same quantum numbers of a right up-type squark in SUSY, therefore it will share its same production mechanisms at colliders. To our knowledge, the closest searches to our scenario that have been performed are those involving squark decays into diquarks, through R-parity violating (RPV) couplings. Constraints on top squarks decaying through RPV couplings were first set by the ALEPH experiment at LEP [93], excluding at 95% CL masses below 75 GeV via four-jet searches. More stringent bounds come from further searches performed by CDF at Tevatron [94] and by ATLAS [95] and CMS [96] at the LHC. The combination of these searches rules out top squarks with RPV decay in the 45 GeV $< M_\Delta <$ 770 GeV interval. All these searches aim to detect four jets in the final state associated to the decay of pair produced heavy resonances. This is the typical signature that one would expect associated with Δ, as for the allowed values of its mass and coupling constants it would decay promptly in the detector. However, as the diquark and leptoquark couplings of Δ are expected to be of the same size, some significant branching ratio of Δ scalar could reside in the $u\,\chi$ channel, such that the signal would be different than the one assumed in four-jet searches, and the limits would change. Performing a detailed collider study of the Δ's, depending on their branching rations into two-jet and one-jets plus missing energy, is beyond the scope of our work, so for definiteness we use the constraints that assume Δ to dominantly decay into two jets.

### 4.4.2 Neutron electric dipole moment

As we have seen in the previous section, the new fields Δ_i and χ contain new sources of CP violation and therefore give rise to new contributions to the neutron electric dipole moment (nEDM). The experimental bound set by the nEDM collaboration at the Paul Scherrer Institut is given by $|d_n| < 1.8 \times 10^{-26} e \cdot cm$ [97]. In this section we analyze the impact of this bound on our model and show that it does not place further significant constraints on the parameter space.

In an EFT approach the electromagnetic moments of a fermion ψ can be described by the effective Lagrangian

$$\mathcal{L}^{\text{eff}} = c_R \overline{\psi} \sigma_{\mu\nu} P_R \psi F^{\mu\nu} + \text{h.c.,} \qquad \text{where} \qquad d = i(c_R - c_R^*) = -2 \operatorname{Im} c_R \qquad (4.15)$$

is the EDM of ψ and $F_{\mu\nu}$ is the field strength tensor of the photon. The diagrams which may give a non-vanishing contribution to the nEDM must have an imaginary component. In general the amplitude of any loop diagram can be recasted as a sum of amplitudes each coming by operators O_i weighted by their coefficients C_i, which can be written as $C = y\,F$. In this notation y stands for the product of the couplings of all the vertices and F is a function coming from the loop integration [98]. In principle both y and F are allowed to be complex, but diagrams with the heavy Δ and χ running in the loop cannot have all the intermediate states go on-shell. Therefore the optical theorem implies that $\operatorname{Im}(F) = 0$ and only y can be complex. Moreover, any combination of couplings entering the expression of the nEDM should be invariant under rephasing of the fields, thus we need at least 4 couplings involving the new BSM states, because $Y = y_{d1}^* y_{u1} y_{u2}^* y_{d2}$ is the simplest combination of the Yukawas with at least one physical phase. As a consequence one needs to go at least to 2-loop to find a possible non-zero contribution.
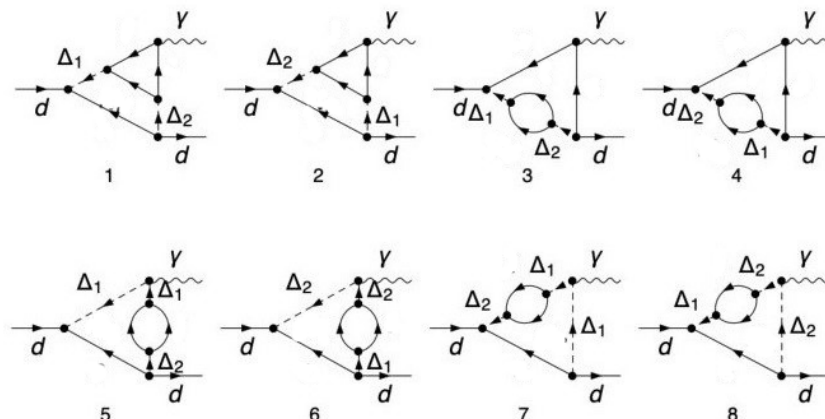
Figure 4. Relevant topologies at two loops for the nEDM. Several contributions for each topology occur due to flavour. While diagrams in the upper row are manifestly symmetric under $\Delta_1 \leftrightarrow \Delta_2$ exchange, a more careful analysis is needed to show the cancellation among the diagrams in the lower row, which is non-trivial due to the different number of Δ_i propagators involved when the photon is attached to an internal Δ leg.

The relevant topologies of our model are depicted in figure 4, they include the Barr-Zee diagrams [99]. They all give in principle non-zero contributions to the nEDM. However, for each of them one can always take the contribution of the 'mirrored' diagram, with complex-conjugate Yukawa couplings and with the photon attached to the same type of field. One can decompose the sum of each set of conjugate diagrams as

$$\sum_{j=1}^{\#\text{conj.}} \mathcal{A}_j = Y F(M_{\Delta_1}, M_{\Delta_2}) + Y^* F(M_{\Delta_2}, M_{\Delta_1}), \tag{4.16}$$

where $F(i, j)$ is coming from the loop integration. $F(i, j)$ is not generically a symmetric function of the scalar masses, but the asymmetry scales like $F(M_{\Delta_2}, M_{\Delta_1}) = F(M_{\Delta_1}, M_{\Delta_2})(1 + \mathcal{O}(k^2/M_{\Delta_{1,2}}^2))$, therefore it vanishes in the $k^2 = 0$ limit for which the nEDM is measured. An explicit proof of this statement is given in the appendix A. Therefore the sum in eq. (4.16) ends up to be real and thus 2-loop diagrams do not produce a non-vanishing nEDM.

At the 3-loop level one expects the dominant contributions to the EDMs to scale as

$$d \sim \frac{y^2 g^4}{(16\pi^2)^3} \times \text{CKM} \times \frac{m_t}{M_\Delta^2} \simeq \frac{10^{-11}}{\text{TeV}} \left(\frac{y}{0.1}\right)^2 \left(\frac{\text{TeV}}{M_\Delta}\right)^2 \frac{\text{CKM}}{0.1}, \tag{4.17}$$

where m_t is the top-quark mass, g is the weak gauge coupling and by 'CKM' we mean a combination of non-diagonal elements of the CKM matrix, which is unavoidable to ensure CP violation and is smaller than at least 0.1. Since limits on coefficients of quarks EDMs (and also CEDMs, for which the discussion is analogous) are in the ballpark of $10^{-9}/\text{TeV}$ (see e.g. [100]) and $M_\Delta \geq \text{TeV}$ from collider bounds, then 3-loop contributions do not give rise to observable EDMs. To conclude, the constraint set by nucleon EDMs on the mass of Δ turns out to be much less stringent than those coming from colliders.
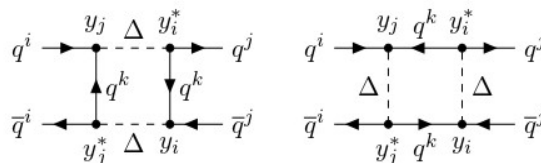
Figure 5. Loop level exchange of Δ contributing to $\Delta F = 2$ transitions.

4.4.3 Flavour violation

Flavour-changing neutral current (FCNC) observables are expected to set powerful constraints on BSM models, due to the non trivial flavour structure that they imply in order to comply with experimental data. In our scenario, $\Delta F = 2$ processes are prohibited at tree level due to the antisymmetric couplings of Δ with the diquarks, which can be parametrized as $y_{ij} = \epsilon_{ijk}y_k$, where i, j, k are flavour indices. These bounds were firstly discussed in [101] and one can identify our state Δ with the diquark denoted as VIII there.

First, it has to be pointed out that the most general flavour structure, with all the flavour off-diagonal couplings switched on, is not needed to account for baryogenesis, as a single non-zero complex coupling is sufficient to provide a physical CP violating phase. In this setup flavour bounds would be evaded completely.

If one wants to stick to the general scenario, bounds coming from the mixing of the neutral K and $B_{d,s}$ mesons have to be taken into account. The Δ scalars then enter the box diagrams in figure 5 and they generate a four-fermion effective Hamiltonian given by

$$H_{\text{eff}}^{NP}(\Delta F = 2) = \frac{1}{32\pi^2}\left(\frac{\lambda_i\lambda_j^*}{M_\Delta^2}\right)G\left(\frac{m_k^2}{M_\Delta^2}\right)(\overline{q_i}\,\gamma^\mu P_R q_j)(\overline{q_i}\gamma_\mu P_R\,q_j)\,, \tag{4.18}$$

where i and j are the external quark flavour indices, $k \neq i \neq j$ is the flavour index of the internal quark, colour indices are contracted within the brackets and the loop function G is given by [101]

$$G(x) = \frac{1 - x^2 + 2\,x\,\log x}{(1 - x)^3}\,. \tag{4.19}$$

Bounds on representative $D = 6$ effective operators contributing to $\Delta F = 2$ transitions have recently been obtained by the UTfit collaboration [102], from a combination of CP conserving and CP violating observables. We can apply these bounds to our model, results are summarised in table 1. Other constraints which we include in table 1 are those associated to the $\Delta F = 1$ processes $b \to s\gamma$, $b \to d\gamma$, R_b and $B^\pm \to \phi\pi^\pm$. We refer to [101] for more details as the constraints reported there can be easily translated to our notation.

One can note that even the most constraining observable, namely ϵ_k, is compatible with Δ diquark couplings of $\mathcal{O}(0.01)$ around the TeV scale, which, in the absence of major hierarchies in the Yukawa couplings, is the benchmark for our baryogenesis mechanism to work. Therefore, we don't expect flavour physics to exclude values of M_Δ that are not already excluded by collider searches. In fact, even assuming a hierarchy of the type $y_{ui} \gg y_{di}$, in order to lower the bound on M_Δ from colliders, one would get at the same time weaker bounds from flavour.

Observable	Bound/(M_Δ/TeV)
ϵ_K	$|\operatorname{Im}(y_1 y_2^*)| \leq 7.8 \times 10^{-4}$
Δm_K	$|\operatorname{Re}(y_1 y_2^*)| \leq 1.4 \times 10^{-2}$
B_d mixing	$|y_1 y_3^*| \leq 1.7 \times 10^{-2}$
B_s mixing	$|y_2 y_3^*| \leq 5.8 \times 10^{-2}$
$b \to s\gamma$	$|y_2 y_3^*| \leq 2.5$
$b \to d\gamma$	$|y_1 y_3^*| \leq 1.2$
R_b	$|y_{1,2}| \leq 24$
$B^\pm \to \phi\pi^\pm$	$|y_1 y_3^*| \leq 3.6 \times 10^{-3}$

Table 1. Bounds in units of M_Δ/TeV on antisymmetrically coupled diquarks.

To conclude, the scalar realisation of our baryogenesis framework may well show-up in current and near-future flavour experiments, but the non-observation of flavour or *CP*-violation there would only exclude some very specific choices of its parameters and not preclude the realisation of baryogenesis.

4.5 Summary of the results

We summarize our results in the plots of figure 6. We have chosen two different benchmark values for $y = \{0.01, 0.1\}$ and $T_{\text{nuc}}/f = \{10^{-3}, 10^{-4}\}$, $M_{\Delta_1} = 4\pi f$ and the dilaton wavefunction normalization $Z = 1$. We compute at each point the boost factor at bubbles collision γ_{coll} using eq. (2.8) and we set $M_{\Delta_2} = 1.2\, M_{\Delta_1}$, $g_{\text{TC}} = 80$, $g_{\text{RH}} = 107.75$ ($= g_{\text{SM}} + 1$, where the $+1$ accounts for the dilaton) and $g_* = g_{\text{TC}} + g_{\text{SM}}$. We saturate the baryon yield at each point, $Y_B/Y_B^{\text{obs}} = 1$, by obtaining $Br(\text{hadr} \to \Delta)$ from eq. (2.12). As anticipated in section 2 we see that Y_B gets suppressed in the runaway regime, hence the allowed parameter space closes at large f and/or small T_{nuc}/f. Values of f lower than the weak scale, for large c_{vac}, cannot be reached due to washout effects. Δ annihilations before decays instead turn out to not constrain our parameter space, for the values of the parameters that we have chosen.

We also display in figure 6 collider bounds, discussed in section 4.4.1, and the expected LISA and ET sensitivities to the GW signal from the PT, discussed in section 3, where to avoid clutter we display only those that include astrophysical foregrounds. By comparing our plots with figure 6 of [36], we see that our scenario extends the allowed parameter space by many order of magnitudes towards smaller values of M_Δ, allowing the PT to occur down to the electroweak scale, potentially in reach of LISA and the Einstein Telescope, and making the mechanism testable at the LHC.

5 Model 2: leptogenesis from a composite sterile neutrino

5.1 Model, neutrino masses and the baryon asymmetry

We now apply our framework for the generation of the baryon asymmetry, based on a supercooled confining PT, to a different model where the observed BAU is sourced via
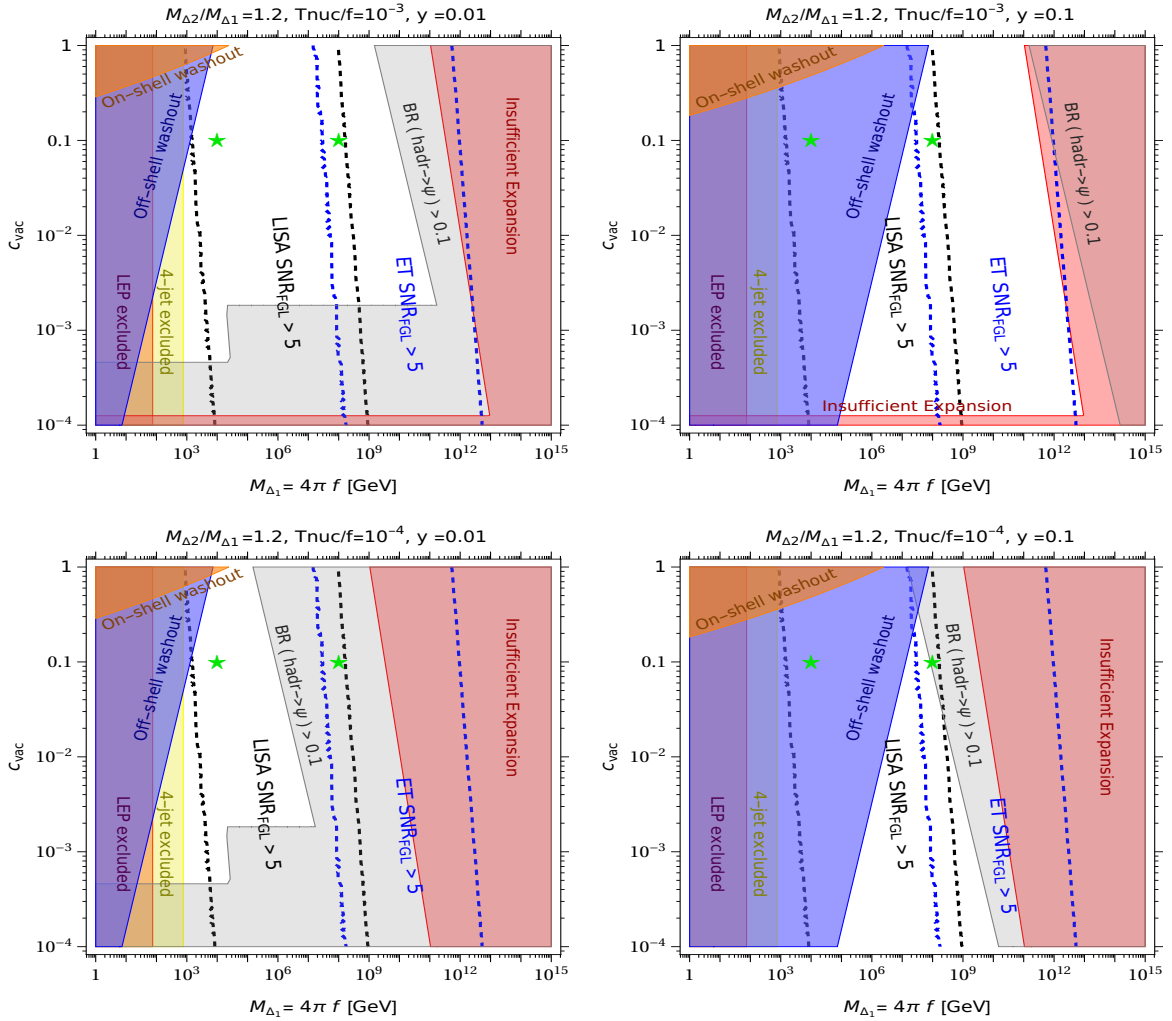
Figure 6. Parameter space for the composite scalar realisation of our framework, which realises baryogenesis. We choose $g_{\rm TC} = 80$, $g_* = g_{\rm SM} + g_{\rm TC}$, $g_{\rm RH} = g_{\rm SM} + 1$ and $Z = 1$ for definiteness. The white area is allowed and accommodates the observed baryon asymmetry, the red and gray regions are excluded by the PT dynamics, as in figure 1. We find that Δ annihilations are slower than Δ decays in the entire parameter space we plot, hence our computation of the BAU is always valid. A value of y smaller than unity is needed to avoid washout. Off-shell and on-shell washout regions are shaded to exclude parameter space where, respectively, $2 \to 2$ interactions eq. (4.7) and inverse decays eq. (4.9) are in equilibrium. Constraints from collider experiments include LEP searches, excluding values of $M_\Delta < 75$ GeV and four-jet searches performed at Tevatron and at the LHC, excluding Δ in the 50 GeV $< M_\Delta < 770$ GeV range. We also show the parameter space testable by the Einstein Telescope (ET) and LISA using $\alpha_{\rm GW} = 100$, $\beta/H = 15$, where the astrophysical foregrounds have been taken into account. We denote with red stars the two points of the parameter space for which we computed the gravitational wave spectrum shown in figure 2.

leptogenesis [103] through the decays of composite sterile neutrinos, which in addition provide mass to the SM neutrinos via a seesaw mechanism. This way we both substantiate the statement that our framework is more general than its specific realisations, and we find results that are interesting for leptogenesis per-se.

We introduce the sterile neutrinos N_a (and denote their two two-component spinors as N_{aL} and N_{aR}) as hadrons of the confining sector, that is responsible for their Dirac mass $M_{N_a} \sim \mathcal{O}(\pi f)$. We then assume that a portal between the confining sector and the SM breaks the SM lepton number, generating inverse seesaw [104, 105] (ISS) as

$$-\mathcal{L}^{\mathrm{ISS}} = y_{a\alpha}\overline{N}_{aR}HL_\alpha + M_{N_a}\overline{N}_aN_a + \frac{\mu_{ab}}{2}\overline{N}_{aL}^c\, N_{bL} + \text{h.c.}, \tag{5.1}$$

where L are the left-handed SM leptons, $\alpha = \{e, \mu, \tau\}$, y is the Yukawa coupling matrix between active and sterile neutrinos, μ is a lepton number breaking Majorana mass matrix, where we further denote by μ_a $(\overline{\mu})$ its complex diagonal (off-diagonal) entries. The presence of μ induces at low energies the $d = 5$ Weinberg operator [106]

$$\delta\mathcal{L}^{d=5} = c_{\alpha\beta}^{d=5}\left(\overline{L_\alpha^c}\,\tilde{H}^*\right)\left(\tilde{H}^\dagger L_\beta\right), \tag{5.2}$$

where $\tilde{H} = i\sigma_2 H^*$ and

$$c_{\alpha\beta}^{d=5} = \left(y^T \frac{1}{M_N^T}\mu\frac{1}{M_N}y\right)_{\alpha\beta}. \tag{5.3}$$

Upon electroweak symmetry breaking, the mass matrix m_ν for the light neutrinos is given by

$$m_\nu = \frac{v^2}{2}y^T M_N^{T-1}\mu M_N^{-1}y\,, \tag{5.4}$$

one can thus express $\mu = \mu(f)$ for a fixed value of the Yukawa coupling y, assuming m_ν to be of the order of the atmospheric neutrino mass, $m_\nu \sim 0.05\,\text{eV}$.

We now assume the heavy Dirac states N_a to come in two generations, which is the minimum number needed to comply with neutrino oscillations data. Without loss of generality, we choose a basis where M_N is diagonal and real. In the non confining ISS the parameter μ is technically small but the hierarchy $\mu \ll M_N$ is not set by any concrete theoretical justification. The latter is instead naturally justified in our setup of composite sterile fermions. One can indeed envisage the possibility that, while the Dirac mass M_N originates from the confining sector, the Majorana one μ originates from physics external to the confining sector, offering a natural way to accomodate $\mu \ll M_N$. An explicit realization is provided in [107], where the strong dynamics is that of a conformal sector deformed by a relevant operator so that it confines in the IR (giving rise to the Dirac masses M_N), and by another operator with different scaling dimension and a small coefficient that gives rise to $\mu \ll M_N$. As anticipated in section 2, our framework also leads to the expectations $\Delta M \equiv |M_{N_2} - M_{N_1}| \ll M_{N_1}$, because the N's are all hadrons of the same sector, as well as $y_{a\alpha} \ll 1$, because the Yukawas originate from a portal.

Therefore, under the natural assumption that $\mu_a \sim \overline{\mu} \sim \mu \ll M_{N_{1,2}}, \Delta M$, one can diagonalize the sterile neutrinos mass matrix to first order in $\delta_a = \mu/M_{N_a}$. Defining four Majorana states $\tilde{N}_i$, $i = 1, 2, 3, 4$, with masses M_i, we have

$$-\mathcal{L}_{\mathrm{mass}}^{\mathrm{ISS}} \supset h_{i\alpha}\overline{\tilde{N}}_i HL_\alpha + \frac{1}{2}M_i\overline{\tilde{N}}_i\tilde{N}_i + \text{h.c.}. \tag{5.5}$$

To first order in δ_a their masses and couplings are given by [108]

$$M_1 \simeq M_{N_1}\Big(1 - \frac{\delta_1}{2}\Big), \qquad h_{1\alpha} \simeq \frac{i}{\sqrt{2}}\Big(y_{1\alpha} + \frac{\delta_1}{4}y_{1\alpha} + \overline{\delta}_1 y_{2\alpha}\Big)$$

$$M_2 \simeq M_{N_1}\Big(1 + \frac{\delta_1}{2}\Big), \qquad h_{2\alpha} \simeq \frac{1}{\sqrt{2}}\Big(y_{1\alpha} - \frac{\delta_1}{4}y_{1\alpha} - \overline{\delta}_1 y_{2\alpha}\Big)$$

$$M_3 \simeq M_{N_2}\Big(1 - \frac{\delta_2}{2}\Big), \qquad h_{3\alpha} \simeq \frac{i}{\sqrt{2}}\Big(y_{2\alpha} + \frac{\delta_2}{4}y_{2\alpha} - \overline{\delta}_2 y_{1\alpha}\Big) \qquad (5.6)$$

$$M_4 \simeq M_{N_2}\Big(1 + \frac{\delta_2}{2}\Big), \qquad h_{4\alpha} \simeq \frac{1}{\sqrt{2}}\Big(y_{2\alpha} - \frac{\delta_2}{4}y_{2\alpha} + \overline{\delta}_2 y_{1\alpha}\Big)$$

where we defined

$$\overline{\delta}_i = \frac{\overline{\mu} M_{N_i}}{M_{N_2}^2 - M_{N_1}^2}\,. \qquad (5.7)$$

Therefore we can see from eq. (5.6) that the heavy neutrinos form pseudo-Dirac pairs with small Majorana splitting controlled by μ/M_{N_i}.

The CP asymmetry generated by the decays of the sterile neutrino N_a then reads

$$\epsilon_a \equiv \frac{\sum_\alpha \Big[\Gamma\Big(N_a \to \ell_\alpha H\Big) - \Gamma\Big(N_a \to \overline{\ell_\alpha} H^*\Big)\Big]}{\sum_\alpha \Big[\Gamma\Big(N_a \to \ell_\alpha H\Big) + \Gamma\Big(N_a \to \overline{\ell_\alpha} H^*\Big)\Big]} = \frac{1}{8\pi}\sum_{j\neq i}\frac{\text{Im}[(hh^\dagger)_{ij}^2}{(hh^\dagger)_{ii}}f_{ij}\,, \qquad (5.8)$$

where we summed over the lepton flavour α in the final state and $f_{ij} \equiv f_{ij}^V + f_{ij}^{\text{self}}$ includes contributions given by vertex and self-energy corrections to the decay, which are given by [109]

$$f_{ij}^V = g\Big(\frac{m_j^2}{m_i^2}\Big), \qquad g(x) = \sqrt{x}\Big[1 - (1+x)\log\frac{x+1}{x}\Big] \qquad (5.9)$$

and [110]

$$f_{ij}^{\text{self}} = \frac{(m_i^2 - m_j^2)m_i m_j}{(m_i^2 - m_j^2)^2 + m_i^2 \Gamma_j^2}, \qquad (5.10)$$

where $\Gamma_i \sim (yy^\dagger)_{ii} M_i/16\pi$ is the decay width of N_i and we assume no hierarchies in masses or couplings among the singlet generations and the SM flavours.

Let us now focus on the ϵ_1 and ϵ_2 contributions to eq. (5.8):

$$\epsilon_1 = \frac{1}{8\pi(hh^\dagger)_{11}}\text{Im}\Big[(hh^\dagger)_{12}^2 f_{12} + (hh^\dagger)_{13}^2 f_{13} + (hh^\dagger)_{14}^2 f_{14}\Big]\,,$$
$$\epsilon_2 = \frac{1}{8\pi(hh^\dagger)_{22}}\text{Im}\Big[(hh^\dagger)_{21}^2 f_{21} + (hh^\dagger)_{23}^2 f_{23} + (hh^\dagger)_{24}^2 f_{24}\Big]\,. \qquad (5.11)$$

Due to the pseudo-Dirac nature of the $(\tilde{N}_1, \tilde{N}_2)$ pair, it follows that

$$(hh^\dagger)_{13}^2 \simeq -(hh^\dagger)_{23}^2 \simeq -(hh^\dagger)_{14}^2 \simeq (hh^\dagger)_{24}^2; \qquad f_{13} \simeq f_{14} \simeq f_{23} \simeq f_{24}. \qquad (5.12)$$

As a consequence, when considering $\epsilon_1 + \epsilon_2$, the f_{12} and f_{21} terms will dominate the sum as those involving f_{i3} and f_{i4} turn out to be of higher order in δ and $\overline{\delta}$ when summed up.
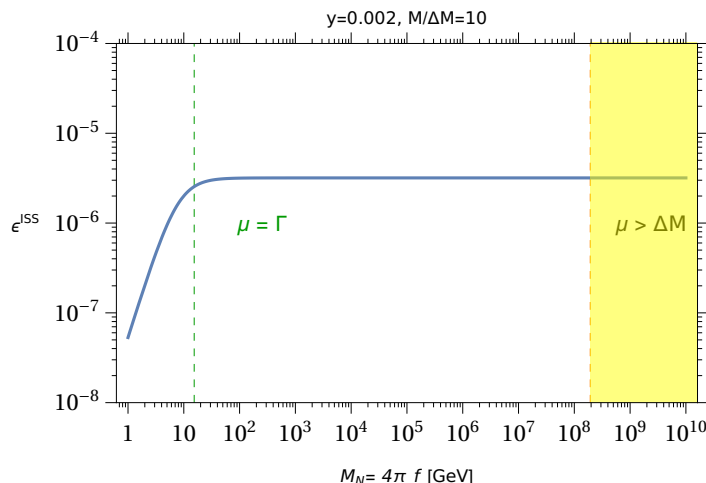
Figure 7. Rate asymmetry ϵ^{ISS} in the inverse see-saw mechanism, obtained from eq. (5.13), for a fixed reference value of the Yukawa coupling $y = 0.002$, a degeneracy $M/\Delta M = 10$ and $\mu = \mu(f)$ fixed by neutrino masses. One can note that an asymptotic value for the produced asymmetry is reached in the $\mu \geq \Gamma$ regime. In the yellow region at large M_N our derivation of eq. (5.13) breaks down, because it assumed $\mu \ll \Delta M$.

An analytical parametric expression for ϵ in the ISS was obtained by the authors of [108], $\epsilon \sim \mu^2/(M_N \Gamma)$, where we dropped the family indices for μ and Γ to show only the parametric dependence. However, the above expression is assuming $\mu \ll \Gamma$, which is not strictly required by the ISS mechanism. We then derive a more general relation that assumes no hierarchy among μ and Γ. In fact as long as $\mu \ll M_N$, ΔM and $\Gamma \ll M_N$, ΔM are satisfied, the dominant one-loop contribution to the rate asymmetry is given by the self energy correction of N, because one has $f_{12}^V - f_{21}^V \sim \delta_1$, therefore the terms involving f_{12}^{self} and $f_{21}^{\text{self}} \simeq -f_{12}^{\text{self}}$ dominate in $\epsilon_1 + \epsilon_2$. We then obtain the total rate asymmetry ϵ^{ISS}

$$\epsilon^{\text{ISS}} \simeq 2(\epsilon_1 + \epsilon_2) \simeq \frac{\text{Im}(yy^\dagger)_{12}}{\pi} \, \overline{\delta}_1 \, f_{12}^{\text{self}} \simeq \frac{\text{Im} y^2}{\pi} \Big(\frac{\mu}{M_N}\Big)^2 \frac{M_N}{\Delta M} \frac{M_N^2}{4\mu^2 + \Gamma^2} \,, \qquad (5.13)$$

where the factor of 2 includes the contribution from $\epsilon_3 + \epsilon_4$, which has the same parametric dependence as the one from $\epsilon_1 + \epsilon_2$. We plot ϵ^{ISS} as a function of $M_N \sim M_{N_{1,2}}$ in figure 7. One can observe from eq. (5.13) that an enhancement of the rate can be obtained in the presence of a quasi-degeneracy among the Dirac masses M_{N_a}. When the two generations $a = 1, 2$ are nearly degenerate, the CP asymmetry is enhanced compared to the non-degenerate case by a factor $M_N/2\Delta M$, as follows from eq. (5.7). We stress that eq. (5.13) holds for $\mu \ll \Delta M$, hence we exclude regions of parameter space where this does not hold from our study. A generalization to the case $\mu \gtrsim \Delta M$ is beyond the scope of this work.

As the baryon asymmetry is now sourced by a lepton asymmetry, one has to require that the reheating temperature, eq. (2.4), is larger than the sphalerons decoupling temperature, $T_{\text{RH}} \geq T_{\text{sph}} \simeq 132 \, \text{GeV}$, in order for the sphalerons to be in thermal equilibrium and therefore to transfer the lepton asymmetry to the baryon sector. Finally, the baryon asymmetry is obtained by plugging ϵ^{ISS} of eq. (5.13) in Y_B of eq. (2.12).

5.2 Washout processes

Following analogous steps to those discussed in the model with the Δ scalar, we now have to take into account washout effects of the lepton number produced at T_{RH}. The $2 \to 2$ scattering rate $\ell H \leftrightarrow \bar{\ell} H^*$, mediated by the sterile fermion N, violates lepton number. Therefore its rate must vanish in the $\mu \to 0$ limit and it can be estimated from the coefficient of the Weinberg operator in the ISS, eq. (5.3):

$$\Gamma_{\mathrm{WO}}(\ell H \to \bar{\ell} H^*) \simeq \frac{y^4 T_{\mathrm{RH}}^3 \mu^2}{4\pi M_N^4} \, , \tag{5.14}$$

which presents a μ^2/M_N^2 suppression with respect to the standard Type-I Seesaw one, where one has only one scale $M_N \sim \mu$. We also included a factor of 2 in eq. (5.14) to account for the contributions given by the degenerate neutrinos. Moreover we assume these washouts to be efficient for $T_{\mathrm{RH}} \geq m_H/3$, when a sizable population of H is still present. Anyway the precise value of T_{RH} for the decoupling of washout effects is not crucial as these processes turn out to play a negligible role in our parameter space. In fact this rate does not spoil the lepton number asymmetry produced by the decays of N provided that it is smaller than $H(T_{\mathrm{RH}})$, i.e. if

$$T_{\mathrm{RH}} < \sqrt{\frac{\pi^2}{90}} \frac{\pi v^4 \, g^{*1/2}}{M_{\mathrm{Pl}} \, m_\nu^2} \sim 10^{13} \mathrm{GeV} \, , \tag{5.15}$$

where the dependence of Γ_{WO} on y, μ and M_N has been absorbed into m_ν by using eq. (5.4).

Also the inverse decays processes $\ell H \to N$, $\bar{\ell} H^* \to N$ can lead to a lepton number washout, if they feel lepton number violation. Indeed, if they do, then they distinguish the initial ℓ states from $\bar{\ell}$ ones and convert more ℓ than $\bar{\ell}$ back into N's. We can assume that the lepton asymmetry produced by N decays does not get erased provided that the inverse-decays rate $\Gamma_{ID} \leq H$ at T_{RH}. It was found by the authors of [111] that the small mass splitting between the two states among the heavy pseudo-Dirac N_i leads to a destructive interference between their contributions to Γ_{ID}, which has the effect of suppressing the washouts. This can be parametrized by the suppression factor of the decay width

$$k^{\mathrm{eff}} = \frac{\rho^2}{1 + \sqrt{c}\rho + \rho^2} = \frac{M_N \mu^2}{\Gamma^2 M_N + \mu \Gamma^2 + M_N \mu^2} \, , \tag{5.16}$$

where $\rho \sim \mu/\Gamma$ and $c \sim (\Gamma/M_N)^2$. The quadratic suppression in μ can be again understood from the fact that inverse decays cannot wash out a lepton asymmetry in the lepton conserving limit, hence they should depend on some power of μ in addition to powers of the Yukawa couplings. One can thus estimate Γ_{ID} as

$$\Gamma_{ID} \simeq 2\Gamma \, k^{\mathrm{eff}} \Big(\frac{M_N}{T_{\mathrm{RH}}} \Big)^{3/2} \mathrm{Exp} \Big[-\frac{M_N}{T_{\mathrm{RH}}} \Big] \, , \tag{5.17}$$

where the factor of 2 comes from the fact that both N_1 and N_2 contribute to washout. This means that the rate of the net washout processes $\ell H \to N$, $\bar{\ell} H^* \to N$ at T_{RH} is suppressed by both the Boltzmann factor and the smallness of μ. Therefore, washouts of the lepton asymmetry turns out to be very suppressed.

To summarize we find that, in the model of leptogenesis from inverse-see-saw and composite neutrinos, $2 \to 2$ washout effects are never the leading constraint on the parameter space of our interest, while inverse decays can become an important constraint only if one lifts the Boltzmann suppression by choosing $M_N < 4\pi f$.

### 5.3 Composite sterile neutrinos at colliders and discussion

We are also interested in possible signatures of the sterile fermions N at colliders, coming from their mixing with the active neutrinos. The requirement $T_{\rm RH} > T_{\rm Sph}$ plus $M_N \sim O(\pi f)$ implies $M_N \gtrsim {\rm TeV}$, making a future high-energy muon collider [112, 113] the leading proposed collider to test this picture. The authors of [114] estimated the projected sensitivity of a $\sqrt{s} = 10\,{\rm TeV}$ muon collider with integrated luminosity $10\,{\rm ab}^{-1}$ on the squared mixing angle $|U_\ell|^2$ between the sterile N and the SM neutrino of flavour ℓ. The dominant N-production mechanism is $\mu^+ \mu^- \to N \bar\nu_\mu$, which, being t-channel, is not suppressed at large center-of-mass squared energies s, and the decay mode considered is $N \to W\ell$ which is fully reconstructable and whose branching ratio is approximately independent of U_ℓ.

The best projected sensitivity occurs for the muon flavoured case and reaches $|U_\mu^2| \lesssim 10^{-6}$ for a sterile fermion mass between 1 and 10 TeV, of course it does not extend to larger masses because $\sqrt{s} = 10\,{\rm TeV}$. In the ISS model the active-sterile neutrino mixing is given by $\sin\theta \sim y\,v/(\sqrt{2}M_N)$, hence $|U_\mu^2| = \sin^2\theta \sim y^2 v^2/(2M_N^2)$. Therefore, for fixed y, the sensitivity $|U_\mu^2| \lesssim 10^{-6}$ translates into a lower limit on M_N: lighter values of M_N will be potentially discoverable at a future high-energy muon collider, and our model turns out to be able to reproduce the BAU for those light M_N values, compatibly with all other constraints.

5.4 Summary of the results

We summarize our findings in figure 8, where we set different benchmark values for y, $M_N/\Delta M$, M_N/f and we take $T_{\rm nuc}/f = 10^{-3}$ and $Z = 1$. A remarkable feature of our mechanism is that, as it is manifest from the plots, one can accomplish leptogenesis around few TeV in the ISS scenario, while this is not the case for the standard thermal leptogenesis ISS scenario, where washout effects are active already at $T_{\rm RH} \sim M_N$ and are too strong to accomodate the required asymmetry, even taking into account quasi-degeneracy enhancements of the rate asymmetry, as shown in [108, 115].

One can see that we expect our model to be partially in reach of a 10 TeV muon collider, provided some mass degeneracy exists between the N_i, of $M_N/\Delta M \sim \mathcal{O}(10^2 - 10^3)$ and as expected given they are hadrons from the same confining sector. A detailed analysis would be needed to make this statement more precise, but goes beyond the scope of its work. Coming to testability at lower-energy colliders, we find an obstacle to make our model viable at lower values of f. The obstacle comes from the interplay between N annihilations before decays and the bounds from washout effects and from the electroweak sphalerons. The latter need to be active, placing the absolute lower limit $T_{\rm RH} \gtrsim 132\,{\rm GeV}$, and hence demanding f to be roughly larger than the weak scale. One could then try to bring M_N within reach of lower-energy colliders by choosing $M_N < (<)4\pi f$, but washout effects would then kick-in to close the allowed parameter space, as visible in the figure 8.
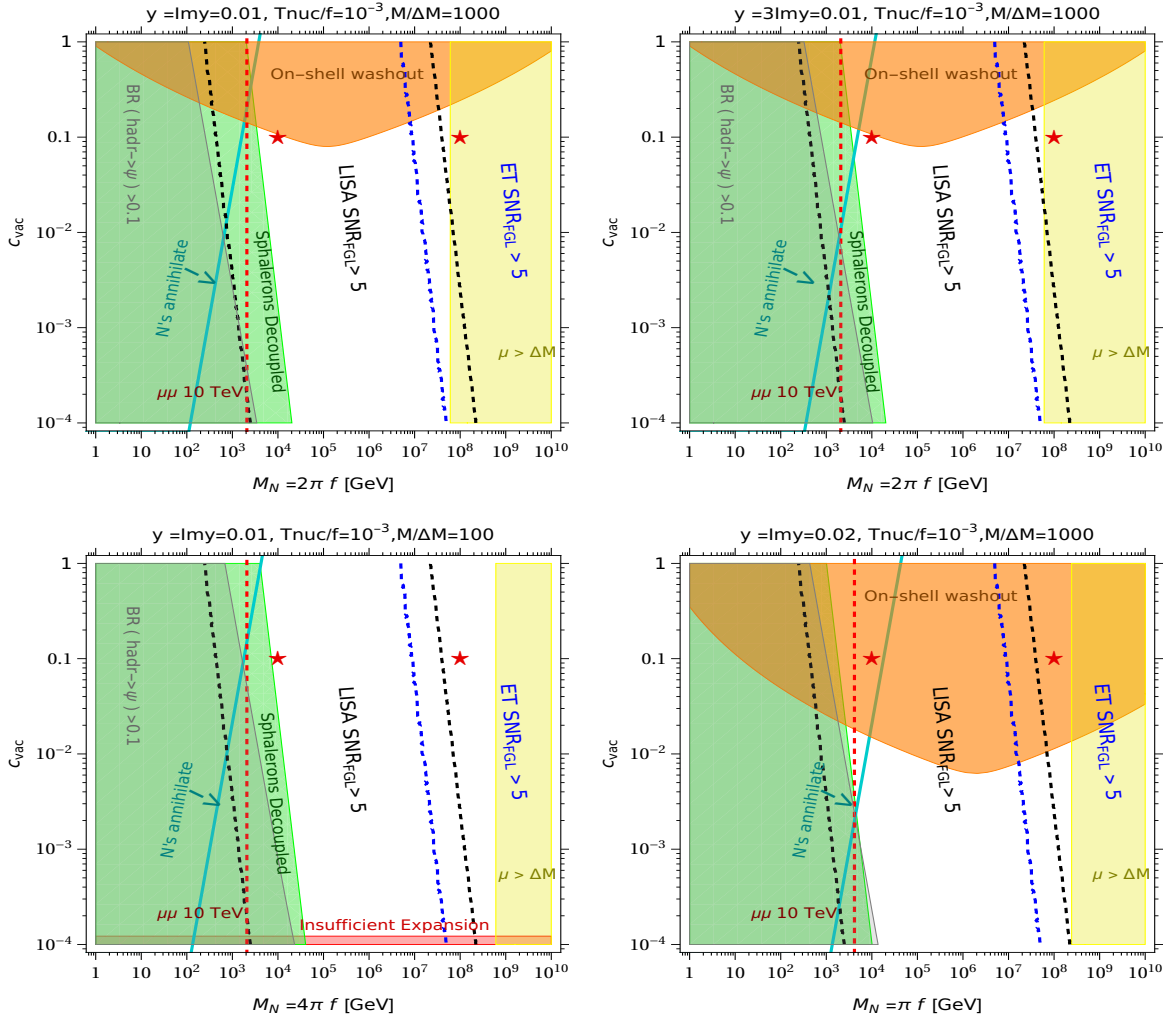
Figure 8. Parameter space for the composite singlet fermion realisation of our framework, which constitutes a variation on inverse see-saw leptogenesis. We choose $g_{\mathrm{TC}} = 80$, $g_* = g_{\mathrm{SM}} + g_{\mathrm{TC}}$, $g_{\mathrm{RH}} = g_{\mathrm{SM}} + 1$ and $Z = 1$ for definiteness. The white area is allowed and accomodates the observed baryon asymmetry, the red and gray regions are excluded by the PT dynamics and above the cyan line the N's start to equilibrate with the dilaton before they decay and our computation of the BAU should be changed, as in figure 1. The dashed red line is obtained from the projected sensitivity of a 10 TeV muon collider on the active-sterile neutrino mixing, see [114]. The green region is excluded from requiring electroweak sphalerons to be out of equilibrium for reheating temperature $T_{\mathrm{RH}} < 132$ GeV. In the orange exclusion regions the on-shell washout processes, i.e. inverse decays of eq. (5.17), are in equilibrium at T_{RH}. The yellow region is excluded by requiring $\mu < \Delta M$ for our expression of the rate asymmetry eq. (5.13) to hold. We also show the parameter space testable by the Einstein Telescope (ET) and LISA using $\alpha_{\mathrm{GW}} = 100$, $\beta/H = 15$, where the astrophysical foregrounds have been taken into account. We denote with red stars the two points of the parameter space for which we computed the gravitational wave spectrum shown in figure 2.

5.5 A comment on linear see-saw

What about other realizations of the seesaw mechanism, like the linear seesaw (LSS)? In analogy to the ISS, additional sterile Dirac fermions N_a are introduced, which mix with the SM neutrinos. In the LSS $\mu = 0$ at tree level and lepton number is explicitly broken by an additional lepton number breaking Yukawa coupling y' of N_{aL} to the SM and we can assume without loss of generality that $y' < y$. The LSS Lagrangian is given by

$$-\mathcal{L}^{\text{LSS}} = y_{a\alpha}\overline{N}_{aR}HL_\alpha + M_{N_a}\overline{N}_aN_a + y'_{a\alpha}\overline{N}^c_{aL}HL_\alpha + \text{h.c.}, \tag{5.18}$$

and the light neutrinos mass matrix reads $m_\nu = v^2(y'^T M_N^{T-1}y + y^T M_N^{-1}y')$. A parametrical expression for the rate asymmetry ϵ^{LSS} was obtained in [108], $\epsilon^{\text{LSS}} \sim y'^2/(16\pi)$. Fixing now y as a function of y' and M_N by using the neutrino mass matrix relation and imposing for consistency that $y' < y$, one obtains an upper bound on y',

$$y' < \Big(\frac{M_N m_\nu}{v^2}\Big)^{1/2} \sim 10^{-6}\Big(\frac{M_N}{\text{TeV}}\Big)^{1/2}, \tag{5.19}$$

which translates into a rate asymmetry $\epsilon^{\text{LSS}} \leq 10^{-12}$ around the TeV scale, way too small to account for the observed baryon yield. Therefore the pure LSS is not a viable model for TeV leptogenesis in our framework.

The discussion above however holds only at tree level. Starting from the pure LSS, a Majorana mass term μ for the N_a is generated at the one-loop level, of the size $\mu \sim M_N yy'/(16\pi^2)$, thus one expects a general LSS+ISS model to arise from a LSS tree level Lagrangian [108]. We may then wonder if a new interesting region of the parameter space opens up in the region where the interference between ISS and LSS contributions produces the relevant term for the rate asymmetry: it turns out that the neutrino mass matrix formula is dominated by the LSS term, while the rate asymmetry by the ISS piece and it reads

$$\epsilon^{\text{LSS+ISS}} = \frac{m_\nu^2 M_N^2}{v^4 y^4}. \tag{5.20}$$

The y coupling needed for leptogenesis, $y \sim \mathcal{O}(10^{-4} - 10^{-5})$ for $M_N \sim \text{TeV}$, is way too small to provide any signatures at colliders, so we will not explore in more detail this model within our supercooled confinement BAU framework.

6 Conclusions and outlook

In this paper we have proposed a new framework for the generation of the observed baryon asymmetry of the universe (BAU), based on a first order supercooled phase transition (PT) of a confining sector. In our framework $B - L$ violating processes are driven by the decays of some composite states (hadrons) of the confined phase. The main advantages with respect to the analogous non-confining mechanism [36] are that in our setup the rate asymmetry is enhanced due to the deep inelastic scatterings occurring upon bubble percolation, which increase the population of the decaying hadrons, and due to the suppression of washout processes because of the hierarchy between the hadron masses and the reheating temperature. Independently of its specific realization, our framework allows to reproduce the observed

BAU down to the weak scale, and potentially down to the MeV one. A first important consequence of this result is that, contrarily to its weakly coupled realisations, the framework is testable in gravitational waves (GWs) not only by the Einstein Telescope but also by lower frequency ones like BDECIGO and LISA. Based on the current understanding of astrophysical foregrounds, the absence of a signal in these experiments will exclude the framework down to the TeV scale, see figure 1.

We have then studied two specific models within our proposed framework, one realising baryogenesis from the decays of composite scalars, charged under the SM, one realising leptogenesis from the decays of composite fermions, singlets under the SM gauge. This allows to include effects that could potentially washout the BAU, to determine other experimental signals, and to possibly connect our framework with open SM problems in addition to the BAU.

◇ Concerning baryogenesis from composite scalars, we have found that washout effects prevent PT scales f lower than a few GeV, see figure 6. We have then studied collider searches for the composite scalars, finding they exclude values of f lower than the weak scale, and that future LHC searches, like 4-jet ones, will test new open territory of this model. The model could also manifest itself in flavour and CP-violating observables, although the size of the effects depends on further details of the model and an absence of deviation from the SM would not exclude it. Finally, we find that the dominant contribution to the neutron EDM arises at 3 loops and the model is not expected to show up there.

◇ Concerning leptogenesis from composite sterile neutrinos, it offers a natural implementation of inverse and linear see-saw scenarios (ISS and LSS), that also explains the small SM neutrino masses. Focusing on the ISS for definiteness, we found that we can reproduce the observed BAU down to scales of the PT $f \sim \text{TeV}$, see figure 8. A degeneracy at the level of 10^{-2} or more is required between the masses of two composite neutrinos, but that is actually expected from a confining sector, while in the standard thermal leptogenesis one generally needs tuning. The obstacle to reach f below the electroweak scale comes from the requirement of a reheating temperature larger than about $130\,\text{GeV}$, so that sphalerons are active. Washout effects are further suppressed, with respect to a generic case, by the insertion of an extra parameter to break lepton number, and only inverse decays can lead to appreciable washout in case $M_N < 4\pi f$. We find that the model is barely testable by N searches at a future muon collider. Our results concerning this model are also interesting from the ISS and LSS points of view, because we enlarge the parameter space where these leptogenesis models work.

Our study opens several interesting avenues of further investigation, both on the model-building and on the phenomenology sides. Concerning the former, it would be for example interesting to connect our framework for the generation of the BAU with solutions to the hierarchy problem of the Fermi scale, given that it works down to the electroweak scale. Concerning phenomenology, it would be interesting to find a specific model realising our framework which allows to go down to the MeV scale for the PT, so to possibly explain the GWs observed by pulsar timing arrays [84–87]. We leave these and other directions for future work.
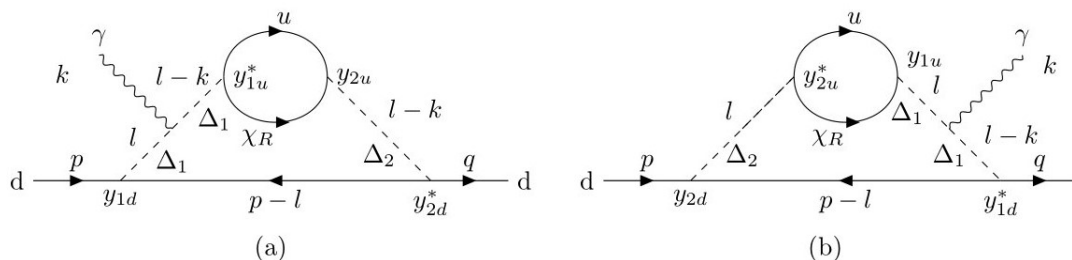
Figure 9. Two-loop conjugate diagrams contributing to the nEDM. In order to obtain a cancellation one needs to take into account also the pair of diagrams where Δ_1 and Δ_2 are interchanged.

A   Cancellation of the 2-loop contributions to the nEDM

Let us show explicitly that the sum of the diagrams shown in figure 9 with in addition those with $\Delta_{1,2}$ swapped provides a vanishing contribution to the nEDM.

The starting point is given by the structure of the electromagnetic nucleon vertex in presence of CP-violation, which is given by

$$i\mathcal{M}^\mu = \overline{u_N}(q)\Big[\gamma^\mu F_E(k^2) + \frac{i\sigma^{\mu\nu}k_\nu}{2m_N}F_M(k^2) + \frac{i\sigma^{\mu\nu}k_\nu}{2m_N}\gamma_5 F_D(k^2)\Big]u_N(p). \tag{A.1}$$

Here $k = (p - q)$ is the momentum of the photon, m_N is the nucleon mass and the EDM of the nucleon is defined as $d_n = F_D(0)/(2m_N)$. Using the Gordon-decomposition of the vector-axial current, the CP violating ($C\!\!\!/P$) part of the above expression reads

$$i\mathcal{M}^\mu_{C\!\!\!/P} = d_n\overline{u_N}(q)\gamma_5 u_N(p)(p+q)^\mu \tag{A.2}$$

Thus we need to concentrate on the $(p + q) \cdot \epsilon$ terms in the computation of the EDM, where ϵ is the photon polarization.

In order to find whether there is a cancellation among the diagrams, we can factor out the upper loop, as it is symmetric under $\Delta_{1,2}$ exchange. Let's focus thus on the lower loop and denote by Y the product of all the Yukawa couplings entering the diagram (a). The relevant amplitude reads

$$\begin{aligned}
iM &= Y \int \frac{d^4\ell}{(2\pi)^4}\overline{u}(q)P_L\frac{i}{\slashed{p}-\slashed{\ell}-m}P_R u(p)\frac{i}{\ell^2-M_1^2}\frac{i}{(\ell-k)^2-M_1^2}\left(\frac{i(2\ell-k)\cdot\epsilon(k)}{(\ell-k)^2-M_2^2}\right) \\
&= Y\overline{u}(q)\gamma^\alpha P_R u(p)\int \frac{d^4\ell}{(2\pi)^4}\frac{(p^\alpha-\ell^\alpha)\ell\cdot\epsilon(k)}{(\ell^2-M_1^2)((\ell-k)^2-M_1^2)((\ell-k)^2-M_2^2)((p-\ell)^2-m^2)}
\end{aligned} \tag{A.3}$$

where m is the mass of the internal quark and $M_{1,2}$ the masses of $\Delta_{1,2}$. Since the Δ_i live at much higher scales than those probed by the EDM we can assume $M_{1,2}^2 \gg k^2, p^2, m^2$. The integrand is dominated by $\ell^2 \sim M_{1,2}^2$, thus one can expand the propagators as

$$\frac{1}{(\ell - k)^2 - M_1^2} \simeq \frac{1}{\ell^2 - M_1^2}\Big[1 + 2\frac{\ell \cdot k}{\ell^2 - M_1^2} + 4\frac{(\ell \cdot k)^2}{(\ell^2 - M_1^2)^2}\Big], \tag{A.4}$$

with analogous expressions for the other propagators. One obtains

$$iM = Y\overline{u}(q)\gamma^\alpha P_R u(p) \int \frac{d^4\ell}{(2\pi)^4} \frac{(p^\alpha - \ell^\alpha)\ell \cdot \epsilon \Big[1 + 2\frac{\ell \cdot k}{\ell^2 - M_1^2} + 4\frac{(\ell \cdot k)^2}{(\ell^2 - M_1^2)^2}\Big]\Big[1 + 2\frac{\ell \cdot k}{\ell^2 - M_2^2} + 4\frac{(\ell \cdot k)^2}{(\ell^2 - M_2^2)^2}\Big]}{\ell^2(l^2 - M_1^2)^2(\ell^2 - M_2^2)}$$
$$\Big[1 + 2\frac{\ell \cdot p}{\ell^2} + 4\frac{(\ell \cdot p)^2}{\ell^4}\Big]$$
$$\tag{A.5}$$

The denominator is now an even function of the loop momentum ℓ, thus we need to focus on terms with an even number of ℓ at numerator. At $\mathcal{O}(\ell^2)$ there are two kind of terms which might contribute to the nEDM,

- $p^\alpha \ell^\mu \ell^\beta p_\beta \epsilon_\mu \sim \ell^2 p^\alpha (p \cdot \epsilon)$

- $p^\alpha \ell^\mu \ell^\beta k_\beta \epsilon_\mu \sim \ell^2 p^\alpha (k \cdot \epsilon) = 0$

and as the non-zero one appears also in diagram (b) the sum of the contribution of (a) and (b) to the nEDM would cancel. Let us consider now $\mathcal{O}(\ell^4)$ terms. There are three types of terms which might contribute:

- $\ell^\alpha \ell^\mu \ell^\beta \ell^\gamma k_\beta k_\gamma \epsilon_\mu \sim (\ell^2)^2\Big[\epsilon_\alpha k^2 + 2 k_\alpha(k \cdot \epsilon)\Big] = 0$

- $\ell^\alpha \ell^\mu \ell^\beta \ell^\gamma p_\beta p_\gamma \epsilon_\mu \sim (\ell^2)^2\Big[\epsilon_\alpha p^2 + 2 p_\alpha(p \cdot \epsilon)\Big]$

- $\ell^\alpha \ell^\mu \ell^\beta \ell^\gamma k_\beta p_\gamma \epsilon_\mu \sim (\ell^2)^2\Big[\epsilon_\alpha(k \cdot p) + p_\alpha(k \cdot \epsilon) + k_\alpha(p \cdot \epsilon)\Big] \sim (\ell^2)^2 k_\alpha(p \cdot \epsilon)$

The second term appears also in the diagram (b) with coefficient Y^* and so it is harmless. The third one receives two contributions from diagram (a), from Δ_1 and Δ_2, while (b) contains only the Δ_1 contribution, as the momentum flowing in Δ_2 doesn't depend on k. Therefore the sum of diagrams (a) and (b) doesn't provide a non-zero nEDM. However, the surviving contribution stems from an integral with a $1/(\ell^2 - M_1^2)^2(\ell^2 - M_2^2)^2$ factor and is cancelled by the couple of conjugate diagrams with $\Delta_{1,2}$ exchanged. We can thus conclude that our model allows new physics contributions to the nEDM to occur only starting at the three loop level.

Open Access. This article is distributed under the terms of the Creative Commons Attribution License (CC-BY4.0), which permits any use, distribution and reproduction in any medium, provided the original author(s) and source are credited.

References

[1] PLANCK collaboration, *Planck 2018 results. VI. Cosmological parameters*, *Astron. Astrophys.* **641** (2020) A6 [*Erratum ibid.* **652** (2021) C4] [`arXiv:1807.06209`] [InSPIRE].

[2] B.D. Fields, K.A. Olive, T.-H. Yeh and C. Young, *Big-Bang Nucleosynthesis after Planck*, *JCAP* **03** (2020) 010 [*Erratum ibid.* **11** (2020) E02] [`arXiv:1912.01132`] [InSPIRE].

[3] A.G. Cohen, A. De Rujula and S.L. Glashow, *A Matter-antimatter universe?*, *Astrophys. J.* **495** (1998) 539 [`astro-ph/9707087`] [InSPIRE].

[4] G. Steigman, *When Clusters Collide: Constraints On Antimatter On The Largest Scales*, *JCAP* **10** (2008) 001 [`arXiv:0808.1122`] [InSPIRE].

[5] E.W. Kolb and M.S. Turner, *The Early Universe*, CRC Press (1990) [`DOI:10.1201/9780429492860`] [InSPIRE].

[6] A.D. Sakharov, *Violation of CP Invariance, C asymmetry, and baryon asymmetry of the universe*, *Pisma Zh. Eksp. Teor. Fiz.* **5** (1967) 32 [InSPIRE].

[7] Y. Aoki et al., *The order of the quantum chromodynamics transition predicted by the standard model of particle physics*, *Nature* **443** (2006) 675 [`hep-lat/0611014`] [InSPIRE].

[8] K. Kajantie, M. Laine, K. Rummukainen and M.E. Shaposhnikov, *Is there a hot electroweak phase transition at $m_H \gtrsim m_W$?*, *Phys. Rev. Lett.* **77** (1996) 2887 [`hep-ph/9605288`] [InSPIRE].

[9] P. Creminelli, A. Nicolis and R. Rattazzi, *Holography and the electroweak phase transition*, *JHEP* **03** (2002) 051 [`hep-th/0107141`] [InSPIRE].

[10] G. Nardini, M. Quiros and A. Wulzer, *A Confining Strong First-Order Electroweak Phase Transition*, *JHEP* **09** (2007) 077 [`arXiv:0706.3388`] [InSPIRE].

[11] T. Konstandin and G. Servant, *Cosmological Consequences of Nearly Conformal Dynamics at the TeV scale*, *JCAP* **12** (2011) 009 [`arXiv:1104.4791`] [InSPIRE].

[12] N. Craig, N. Levi, A. Mariotti and D. Redigolo, *Ripples in Spacetime from Broken Supersymmetry*, *JHEP* **21** (2020) 184 [`arXiv:2011.13949`] [InSPIRE].

[13] R. Jinno and M. Takimoto, *Probing a classically conformal $B - L$ model with gravitational waves*, *Phys. Rev. D* **95** (2017) 015020 [`arXiv:1604.05035`] [InSPIRE].

[14] L. Delle Rose, G. Panico, M. Redi and A. Tesi, *Gravitational Waves from Supercool Axions*, *JHEP* **04** (2020) 025 [`arXiv:1912.06139`] [InSPIRE].

[15] B. Von Harling, A. Pomarol, O. Pujolàs and F. Rompineve, *Peccei-Quinn Phase Transition at LIGO*, *JHEP* **04** (2020) 195 [`arXiv:1912.07587`] [InSPIRE].

[16] A. Greljo, T. Opferkuch and B.A. Stefanek, *Gravitational Imprints of Flavor Hierarchies*, *Phys. Rev. Lett.* **124** (2020) 171802 [`arXiv:1910.02014`] [InSPIRE].

[17] D. Bodeker and W. Buchmuller, *Baryogenesis from the weak scale to the grand unification scale*, *Rev. Mod. Phys.* **93** (2021) 035004 [`arXiv:2009.07294`] [InSPIRE].

[18] E. Witten, *Cosmic Separation of Phases*, *Phys. Rev. D* **30** (1984) 272 [InSPIRE].

[19] C.J. Hogan, *Gravitational radiation from cosmological phase transitions*, *Mon. Not. Roy. Astron. Soc.* **218** (1986) 629.

[20] NANOGRAV collaboration, *The NANOGrav 15 yr Data Set: Search for Signals from New Physics*, *Astrophys. J. Lett.* **951** (2023) L11 [`arXiv:2306.16219`] [InSPIRE].

[21] EPTA collaboration, *The second data release from the European Pulsar Timing Array: V. Implications for massive black holes, dark matter and the early Universe*, `arXiv:2306.16227` [INSPIRE].

[22] Y. Gouttenoire, *First-Order Phase Transition Interpretation of Pulsar Timing Array Signal Is Consistent with Solar-Mass Black Holes*, *Phys. Rev. Lett.* **131** (2023) 171404 [`arXiv:2307.04239`] [INSPIRE].

[23] LISA Cosmology Working Group collaboration, *Cosmology with the Laser Interferometer Space Antenna*, *Living Rev. Rel.* **26** (2023) 5 [`arXiv:2204.05434`] [INSPIRE].

[24] A. Falkowski and J.M. No, *Non-thermal Dark Matter Production from the Electroweak Phase Transition: Multi-TeV WIMPs and 'Baby-Zillas'*, *JHEP* **02** (2013) 034 [`arXiv:1211.5615`] [INSPIRE].

[25] T. Hambye, A. Strumia and D. Teresi, *Super-cool Dark Matter*, *JHEP* **08** (2018) 188 [`arXiv:1805.01473`] [INSPIRE].

[26] I. Baldes, Y. Gouttenoire and F. Sala, *String Fragmentation in Supercooled Confinement and Implications for Dark Matter*, *JHEP* **04** (2021) 278 [`arXiv:2007.08440`] [INSPIRE].

[27] A. Azatov, M. Vanvlasselaer and W. Yin, *Dark Matter production from relativistic bubble walls*, *JHEP* **03** (2021) 288 [`arXiv:2101.05721`] [INSPIRE].

[28] I. Baldes, Y. Gouttenoire and F. Sala, *Hot and heavy dark matter from a weak scale phase transition*, *SciPost Phys.* **14** (2023) 033 [`arXiv:2207.05096`] [INSPIRE].

[29] I. Baldes, M. Dichtl, Y. Gouttenoire and F. Sala, *Bubbletrons*, `arXiv:2306.15555` [INSPIRE].

[30] J. Liu et al., *Primordial black hole production during first-order phase transitions*, *Phys. Rev. D* **105** (2022) L021303 [`arXiv:2106.05637`] [INSPIRE].

[31] K. Hashino, S. Kanemura and T. Takahashi, *Primordial black holes as a probe of strongly first-order electroweak phase transition*, *Phys. Lett. B* **833** (2022) 137261 [`arXiv:2111.13099`] [INSPIRE].

[32] M. Lewicki, P. Toczek and V. Vaskonen, *Primordial black holes from strong first-order phase transitions*, *JHEP* **09** (2023) 092 [`arXiv:2305.04924`] [INSPIRE].

[33] Y. Gouttenoire and T. Volansky, *Primordial Black Holes from Supercooled Phase Transitions*, `arXiv:2305.04942` [INSPIRE].

[34] A. Katz and A. Riotto, *Baryogenesis and Gravitational Waves from Runaway Bubble Collisions*, *JCAP* **11** (2016) 011 [`arXiv:1608.00583`] [INSPIRE].

[35] A. Azatov, M. Vanvlasselaer and W. Yin, *Baryogenesis via relativistic bubble walls*, *JHEP* **10** (2021) 043 [`arXiv:2106.14913`] [INSPIRE].

[36] I. Baldes et al., *Baryogenesis via relativistic bubble expansion*, *Phys. Rev. D* **104** (2021) 115029 [`arXiv:2106.15602`] [INSPIRE].

[37] P. Huang and K.-P. Xie, *Leptogenesis triggered by a first-order phase transition*, *JHEP* **09** (2022) 052 [`arXiv:2206.04691`] [INSPIRE].

[38] E.J. Chun et al., *Bubble-assisted leptogenesis*, *JHEP* **09** (2023) 164 [`arXiv:2305.10759`] [INSPIRE].

[39] M.B. Hindmarsh, M. Lüben, J. Lumma and M. Pauly, *Phase transitions in the early universe*, *SciPost Phys. Lect. Notes* **24** (2021) 1 [`arXiv:2008.09136`] [INSPIRE].

[40] Y. Gouttenoire, *Beyond the Standard Model Cocktail*, Springer, Cham (2022) [DOI:10.1007/978-3-031-11862-3] [INSPIRE].

[41] E. Witten, *Cosmological Consequences of a Light Higgs Boson*, *Nucl. Phys. B* **177** (1981) 477 [INSPIRE].

[42] N. Levi, T. Opferkuch and D. Redigolo, *The supercooling window at weak and strong coupling*, *JHEP* **02** (2023) 125 [arXiv:2212.08085] [INSPIRE].

[43] S.R. Coleman and E.J. Weinberg, *Radiative Corrections as the Origin of Spontaneous Symmetry Breaking*, *Phys. Rev. D* **7** (1973) 1888 [INSPIRE].

[44] E. Gildener and S. Weinberg, *Symmetry Breaking and Scalar Bosons*, *Phys. Rev. D* **13** (1976) 3333 [INSPIRE].

[45] L. Randall and G. Servant, *Gravitational waves from warped spacetime*, *JHEP* **05** (2007) 054 [hep-ph/0607158] [INSPIRE].

[46] I. Baldes, Y. Gouttenoire, F. Sala and G. Servant, *Supercool composite Dark Matter beyond 100 TeV*, *JHEP* **07** (2022) 084 [arXiv:2110.13926] [INSPIRE].

[47] S. Iso, P.D. Serpico and K. Shimada, *QCD-Electroweak First-Order Phase Transition in a Supercooled Universe*, *Phys. Rev. Lett.* **119** (2017) 141301 [arXiv:1704.04955] [INSPIRE].

[48] B. von Harling and G. Servant, *QCD-induced Electroweak Phase Transition*, *JHEP* **01** (2018) 159 [arXiv:1711.11554] [INSPIRE].

[49] R. Contino, A. Pomarol and R. Rattazzi, *The naturally light dilaton or How to break dilations spontaneously and naturally*, unpublished work [https://indico.cern.ch/event/75810/contributions/1250635/attachments/1050757/1498158/Rattazzi.pdf].

[50] T. Appelquist and Y. Bai, *A Light Dilaton in Walking Gauge Theories*, *Phys. Rev. D* **82** (2010) 071701 [arXiv:1006.4375] [INSPIRE].

[51] B. Bellazzini et al., *A Higgslike Dilaton*, *Eur. Phys. J. C* **73** (2013) 2333 [arXiv:1209.3299] [INSPIRE].

[52] F. Coradeschi et al., *A naturally light dilaton*, *JHEP* **11** (2013) 057 [arXiv:1306.4601] [INSPIRE].

[53] Z. Chacko, R.K. Mishra and D. Stolarski, *Dynamics of a Stabilized Radion and Duality*, *JHEP* **09** (2013) 121 [arXiv:1304.1795] [INSPIRE].

[54] E. Megias and O. Pujolàs, *Naturally light dilatons from nearly marginal deformations*, *JHEP* **08** (2014) 081 [arXiv:1401.4998] [INSPIRE].

[55] T. Konstandin and J.M. No, *Hydrodynamic obstruction to bubble expansion*, *JCAP* **02** (2011) 008 [arXiv:1011.3735] [INSPIRE].

[56] B. Laurent and J.M. Cline, *First principles determination of bubble wall velocity*, *Phys. Rev. D* **106** (2022) 023501 [arXiv:2204.13120] [INSPIRE].

[57] D. Bodeker and G.D. Moore, *Can electroweak bubble walls run away?*, *JCAP* **05** (2009) 009 [arXiv:0903.4099] [INSPIRE].

[58] D. Bodeker and G.D. Moore, *Electroweak Bubble Wall Speed Limit*, *JCAP* **05** (2017) 025 [arXiv:1703.08215] [INSPIRE].

[59] Y. Gouttenoire, R. Jinno and F. Sala, *Friction pressure on relativistic bubble walls*, *JHEP* **05** (2022) 004 [arXiv:2112.07686] [INSPIRE].

[60] K. Enqvist, J. Ignatius, K. Kajantie and K. Rummukainen, *Nucleation and bubble growth in a first order cosmological electroweak phase transition*, *Phys. Rev. D* **45** (1992) 3415 [InSPIRE].

[61] I. Baldes and M.O. Olea-Romacho, *Primordial black holes as dark matter: interferometric tests of phase transition origin*, *JHEP* **01** (2024) 133 [arXiv:2307.11639] [InSPIRE].

[62] I. Baldes, M. Dichtl, Y. Gouttenoire and F. Sala, *Particle Shells from Relativistic Bubble Walls*, to appear.

[63] S. Bruggisser, B. Von Harling, O. Matsedonskyi and G. Servant, *Baryon Asymmetry from a Composite Higgs Boson*, *Phys. Rev. Lett.* **121** (2018) 131801 [arXiv:1803.08546] [InSPIRE].

[64] S. Bruggisser, B. von Harling, O. Matsedonskyi and G. Servant, *Status of electroweak baryogenesis in minimal composite Higgs*, *JHEP* **08** (2023) 012 [arXiv:2212.11953] [InSPIRE].

[65] V.A. Kuzmin, V.A. Rubakov and M.E. Shaposhnikov, *On the Anomalous Electroweak Baryon Number Nonconservation in the Early Universe*, *Phys. Lett. B* **155** (1985) 36 [InSPIRE].

[66] S.Y. Khlebnikov and M.E. Shaposhnikov, *The Statistical Theory of Anomalous Fermion Number Nonconservation*, *Nucl. Phys. B* **308** (1988) 885 [InSPIRE].

[67] D. Cutting, E.G. Escartin, M. Hindmarsh and D.J. Weir, *Gravitational waves from vacuum first order phase transitions II: from thin to thick walls*, *Phys. Rev. D* **103** (2021) 023531 [arXiv:2005.13537] [InSPIRE].

[68] R. Durrer and C. Caprini, *Primordial magnetic fields and causality*, *JCAP* **11** (2003) 010 [astro-ph/0305059] [InSPIRE].

[69] C. Caprini et al., *Science with the space-based interferometer eLISA. II: Gravitational waves from cosmological phase transitions*, *JCAP* **04** (2016) 001 [arXiv:1512.06239] [InSPIRE].

[70] C. Caprini et al., *Detecting gravitational waves from cosmological phase transitions with LISA: an update*, *JCAP* **03** (2020) 024 [arXiv:1910.13125] [InSPIRE].

[71] D. Cutting, M. Hindmarsh and D.J. Weir, *Vorticity, kinetic energy, and suppressed gravitational wave production in strong first order phase transitions*, *Phys. Rev. Lett.* **125** (2020) 021302 [arXiv:1906.00480] [InSPIRE].

[72] R. Jinno, H. Seong, M. Takimoto and C.M. Um, *Gravitational waves from first-order phase transitions: Ultra-supercooled transitions and the fate of relativistic shocks*, *JCAP* **10** (2019) 033 [arXiv:1905.00899] [InSPIRE].

[73] T. Konstandin, *Gravitational radiation from a bulk flow model*, *JCAP* **03** (2018) 047 [arXiv:1712.06869] [InSPIRE].

[74] S. Hild et al., *Sensitivity Studies for Third-Generation Gravitational Wave Observatories*, *Class. Quant. Grav.* **28** (2011) 094013 [arXiv:1012.0908] [InSPIRE].

[75] E. Thrane and J.D. Romano, *Sensitivity curves for searches for gravitational-wave backgrounds*, *Phys. Rev. D* **88** (2013) 124032 [arXiv:1310.5300] [InSPIRE].

[76] C. Caprini et al., *Reconstructing the spectral shape of a stochastic gravitational wave background with LISA*, *JCAP* **11** (2019) 017 [arXiv:1906.09244] [InSPIRE].

[77] S. Kawamura et al., *Current status of space gravitational wave antenna DECIGO and B-DECIGO*, *PTEP* **2021** (2021) 05A105 [arXiv:2006.13545] [InSPIRE].

[78] KAGRA et al. collaborations, *Upper limits on the isotropic gravitational-wave background from Advanced LIGO and Advanced Virgo's third observing run*, *Phys. Rev. D* **104** (2021) 022004 [arXiv:2101.12130] [InSPIRE].

[79] M. Branchesi et al., *Science with the Einstein Telescope: a comparison of different designs*, *JCAP* **07** (2023) 068 [`arXiv:2303.15923`] [InSPIRE].

[80] P.A. Rosado, *Gravitational wave background from binary systems*, *Phys. Rev. D* **84** (2011) 084004 [`arXiv:1106.5795`] [InSPIRE].

[81] T. Robson, N.J. Cornish and C. Liu, *The construction and use of LISA sensitivity curves*, *Class. Quant. Grav.* **36** (2019) 105011 [`arXiv:1803.01944`] [InSPIRE].

[82] A.J. Farmer and E.S. Phinney, *The gravitational wave background from cosmological compact binaries*, *Mon. Not. Roy. Astron. Soc.* **346** (2003) 1197 [`astro-ph/0304393`] [InSPIRE].

[83] K. Aggarwal et al., *The NANOGrav 11-Year Data Set: Limits on Gravitational Waves from Individual Supermassive Black Hole Binaries*, *Astrophys. J.* **880** (2019) 2 [`arXiv:1812.11585`] [InSPIRE].

[84] NANOGRAV collaboration, *The NANOGrav 12.5 yr Data Set: Search for an Isotropic Stochastic Gravitational-wave Background*, *Astrophys. J. Lett.* **905** (2020) L34 [`arXiv:2009.04496`] [InSPIRE].

[85] B. Goncharov et al., *On the Evidence for a Common-spectrum Process in the Search for the Nanohertz Gravitational-wave Background with the Parkes Pulsar Timing Array*, *Astrophys. J. Lett.* **917** (2021) L19 [`arXiv:2107.12112`] [InSPIRE].

[86] EPTA collaboration, *Common-red-signal analysis with 24-yr high-precision timing of the European Pulsar Timing Array: inferences in the stochastic gravitational-wave background search*, *Mon. Not. Roy. Astron. Soc.* **508** (2021) 4970 [`arXiv:2110.13184`] [InSPIRE].

[87] J. Antoniadis et al., *The International Pulsar Timing Array second data release: Search for an isotropic gravitational wave background*, *Mon. Not. Roy. Astron. Soc.* **510** (2022) 4873 [`arXiv:2201.03980`] [InSPIRE].

[88] NANOGRAV collaboration, *Searching for Gravitational Waves from Cosmological Phase Transitions with the NANOGrav 12.5-Year Dataset*, *Phys. Rev. Lett.* **127** (2021) 251302 [`arXiv:2104.13930`] [InSPIRE].

[89] T. Bringmann et al., *Does NANOGrav observe a dark sector phase transition?*, *JCAP* **11** (2023) 053 [`arXiv:2306.09411`] [InSPIRE].

[90] R.E. Cutkosky, *Singularities and discontinuities of Feynman amplitudes*, *J. Math. Phys.* **1** (1960) 429 [InSPIRE].

[91] SUPER-KAMIOKANDE collaboration, *Search for proton decay via $p \to \nu K^+$ using* 260 *kiloton · year data of Super-Kamiokande*, *Phys. Rev. D* **90** (2014) 072005 [`arXiv:1408.1195`] [InSPIRE].

[92] ALEPH et al. collaborations, *Precision electroweak measurements on the Z resonance*, *Phys. Rept.* **427** (2006) 257 [`hep-ex/0509008`] [InSPIRE].

[93] ALEPH collaboration, *Search for supersymmetric particles with R parity violating decays in e^+e^- collisions at $\sqrt{s}$ up to* 209-*GeV*, *Eur. Phys. J. C* **31** (2003) 1 [`hep-ex/0210014`] [InSPIRE].

[94] CDF collaboration, *Search for Pair Production of Strongly Interacting Particles Decaying to Pairs of Jets in $p\bar{p}$ Collisions at $\sqrt{s} = 1.96$ TeV*, *Phys. Rev. Lett.* **111** (2013) 031802 [`arXiv:1303.2699`] [InSPIRE].

[95] ATLAS collaboration, *A search for pair-produced resonances in four-jet final states at $\sqrt{s} = 13$ TeV with the ATLAS detector*, *Eur. Phys. J. C* **78** (2018) 250 [`arXiv:1710.07171`] [InSPIRE].

[96] CMS collaboration, *Search for resonant and nonresonant production of pairs of dijet resonances in proton-proton collisions at $\sqrt{s} = 13$ TeV*, *JHEP* **07** (2023) 161 [arXiv:2206.09997] [ɪɴSPIRE].

[97] C. Abel et al., *Measurement of the Permanent Electric Dipole Moment of the Neutron*, *Phys. Rev. Lett.* **124** (2020) 081803 [arXiv:2001.11966] [ɪɴSPIRE].

[98] W. Bensalem and D. Stolarski, *Flavor and CP violation from a QCD-like hidden sector*, *JHEP* **02** (2022) 011 [arXiv:2111.05515] [ɪɴSPIRE].

[99] S.M. Barr and A. Zee, *Electric Dipole Moment of the Electron and of the Neutron*, *Phys. Rev. Lett.* **65** (1990) 21 [*Erratum ibid.* **65** (1990) 2920] [ɪɴSPIRE].

[100] F. Sala, *A bound on the charm chromo-EDM and its implications*, *JHEP* **03** (2014) 061 [arXiv:1312.2589] [ɪɴSPIRE].

[101] G.F. Giudice, B. Gripaios and R. Sundrum, *Flavourful Production at Hadron Colliders*, *JHEP* **08** (2011) 055 [arXiv:1105.3161] [ɪɴSPIRE].

[102] M. Bona et al., *Unitarity Triangle global fits beyond the Standard Model: UTfit 2021 NP update*, *PoS* **EPS-HEP2021** (2022) 500 [ɪɴSPIRE].

[103] M. Fukugita and T. Yanagida, *Baryogenesis Without Grand Unification*, *Phys. Lett. B* **174** (1986) 45 [ɪɴSPIRE].

[104] R.N. Mohapatra, *Mechanism for Understanding Small Neutrino Mass in Superstring Theories*, *Phys. Rev. Lett.* **56** (1986) 561 [ɪɴSPIRE].

[105] R.N. Mohapatra and J.W.F. Valle, *Neutrino Mass and Baryon Number Nonconservation in Superstring Models*, *Phys. Rev. D* **34** (1986) 1642 [ɪɴSPIRE].

[106] S. Weinberg, *Baryon and Lepton Nonconserving Processes*, *Phys. Rev. Lett.* **43** (1979) 1566 [ɪɴSPIRE].

[107] Z. Chacko, P.J. Fox, R. Harnik and Z. Liu, *Neutrino Masses from Low Scale Partial Compositeness*, *JHEP* **03** (2021) 112 [arXiv:2012.01443] [ɪɴSPIRE].

[108] K. Agashe et al., *Natural Seesaw and Leptogenesis from Hybrid of High-Scale Type I and TeV-Scale Inverse*, *JHEP* **04** (2019) 029 [arXiv:1812.08204] [ɪɴSPIRE].

[109] L. Covi, E. Roulet and F. Vissani, *CP violating decays in leptogenesis scenarios*, *Phys. Lett. B* **384** (1996) 169 [hep-ph/9605319] [ɪɴSPIRE].

[110] F.F. Deppisch and A. Pilaftsis, *Lepton Flavour Violation and θ_{13} in Minimal Resonant Leptogenesis*, *Phys. Rev. D* **83** (2011) 076007 [arXiv:1012.1834] [ɪɴSPIRE].

[111] S. Blanchet, T. Hambye and F.-X. Josse-Michaux, *Reconciling leptogenesis with observable $\mu \to e\gamma$ rates*, *JHEP* **04** (2010) 023 [arXiv:0912.3153] [ɪɴSPIRE].

[112] H. Al Ali et al., *The muon Smasher's guide*, *Rept. Prog. Phys.* **85** (2022) 084201 [arXiv:2103.14043] [ɪɴSPIRE].

[113] C. Aime et al., *Muon Collider Physics Summary*, arXiv:2203.07256 [ɪɴSPIRE].

[114] P. Li, Z. Liu and K.-F. Lyu, *Heavy neutral leptons at muon colliders*, *JHEP* **03** (2023) 231 [arXiv:2301.07117] [ɪɴSPIRE].

[115] M.J. Dolan, T.P. Dutka and R.R. Volkas, *Dirac-Phase Thermal Leptogenesis in the extended Type-I Seesaw Model*, *JCAP* **06** (2018) 012 [arXiv:1802.08373] [ɪɴSPIRE].